

Our Reference: UMJ-116-E (UM-2172p3)

PATENT

## **SELECTIVE SORBENTS FOR PURIFICATION OF HYDROCARBONS**

### **CROSS REFERENCE TO RELATED APPLICATIONS**

This application is a continuation-in-part of U.S. Application Serial No. 10/613,131, filed July 3, 2003, which is itself a continuation-in-part of U.S. Application Serial No. 10/393,962, filed March 21, 2003, which is itself a continuation-in-part of U.S. Application Serial No. 10/234,681, filed September 4, 2002, which itself claims benefit of U.S. Provisional Patent application Serial No. 60/317,158, filed September 4, 2001.

### **STATEMENT REGARDING FEDERALLY SPONSORED RESEARCH OR DEVELOPMENT**

This invention was made in the course of research partially supported by a grant from the National Science Foundation (NSF) (Grant No. CTS-9819008 and Grant No. CTS-0138190); and by a grant from the Department of Energy (DOE) (Fuel Cell Grant No. DE-FC04-02AL67630). The U.S. government has certain rights in the invention.

### **BACKGROUND OF THE INVENTION**

The present invention relates generally to processes for purification of hydrocarbons and, more particularly, to adsorption processes using sorbents selective to sulfur compounds and to aromatic compounds.

Petroleum is an extremely complex mixture and consists predominantly of hydrocarbons, as well as compounds containing nitrogen, oxygen, and sulfur. Most petroleums also contain minor amounts of nickel and vanadium. The chemical and physical properties of petroleum vary considerably because of the variations in composition.

The ultimate analysis (elemental composition) of petroleum tends to vary over relatively narrow limits -- carbon: 83.0 to 87.0 percent; hydrogen: 10.0 to 14.0 percent; nitrogen: 0.1 to 1.5 percent; oxygen: 0.1 to 1.5 percent; sulfur: 0.1 to 5.0 percent; metals (nickel plus vanadium): 10 to 500 ppm.

Crude oils are seldom used as fuel because they are more valuable when refined to petroleum products. Distillation separates the crude oil into fractions equivalent in boiling range to gasoline, kerosene, gas oil, lubricating oil, and residual. Thermal or catalytic cracking is used to convert kerosene, gas oil, or residual to gasoline, lower-boiling fractions, and a residual coke. Petrochemical intermediates such as ethylene and propylene are primarily produced by the thermal cracking of light hydrocarbon feedstocks

in the presence of steam. Catalytic reforming, isomerization, alkylation, polymerization, hydrogenation, and combinations of these catalytic processes are used to upgrade the various refinery intermediates into improved gasoline stocks or distillates. The major finished products are usually blends of a number of stocks, plus additives.

5 Gasoline is a complex mixture of hydrocarbons that distills within the range 100 to 400°F. Commercial gasolines are blends of straight-run, cracked, reformed, and natural gasolines. Straight-run gasoline is recovered from crude petroleum by distillation and contains a large proportion of normal hydrocarbons of the paraffin series. Cracked gasoline is manufactured by heating crude-petroleum distillation fractions or residues  
10 under pressure, or by heating with or without pressure in the presence of a catalyst. Heavier hydrocarbons are broken into smaller molecules, some of which distill in the gasoline range. Reformed gasoline is made by passing gasoline fractions over catalysts in such a manner that low-octane-number hydrocarbons are molecularly rearranged to high-octane-number components. Many of the catalysts use platinum and other metals  
15 deposited on a silica and/or alumina support. Natural gasoline is obtained from natural gas by liquefying those constituents which boil in the gasoline range either by compression and cooling or by absorption in oil.

Removal of the sulfur-containing compounds is an important operation in petroleum refining, and is often achieved by catalytic processes at elevated temperatures  
20 and pressures. The hydrosulfurization (HDS) process is efficient in removing thiols and sulfides, but much less effective for heterocyclic diunsaturated sulfur compounds, such as thiophenes and thiophene compounds/derivatives (e.g., benzothiophene and dibenzothiophene).

In 1998, the U.S. largest automakers pledged to put clean-burning cars on  
25 the road by 2001, beating the Clean Air Act Amendments mandate by five years. They proposed the use of internal combustion (IC) engines capable of emitting 50% fewer nitrogen oxides (NO<sub>x</sub>) and 70% fewer hydrocarbons, thanks to advanced catalytic converters. Shortly after this low-emission vehicle concept was announced, the U.S. Environmental Protection Agency (EPA) revealed concerns that these reductions might not  
30 be achievable if high-sulfur gasoline and diesel fuel continue to be used. Studies involving the EPA and the automobile and oil industries showed that fuel sulfur atoms can bond with reactive sites on the catalyst surface, preventing catalyzed reactions needed to break down NO<sub>x</sub> and hydrocarbons. Since high-sulfur gasoline may perhaps decrease the effectiveness of advanced catalytic converters, the EPA mandates a reduction in gasoline and diesel  
35 sulfur levels to 30 and 15 ppm, respectively, down from the current levels of 300-500 ppm. This should be attained by the year 2006. Faced with the severely high costs of

compliance, a surprising number of refiners are seriously considering reducing or eliminating production of on-board fuels.

Ultra-clean fuel may also be desirable for use with a fuel cell system. For the automotive fuel cells, liquid hydrocarbons may be ideal fuels due to their higher energy density, availability, and safety for transportation and storage. However, liquid hydrocarbons usually contain certain sulfur compounds that are poisonous to both the shift catalysts in the hydrocarbon fuel processors and the electrode catalysts in fuel cell processes. Thus, the sulfur content in the liquid hydrocarbons would desirably be generally less than about 0.1 ppm.

During the last decade, there have been several published accounts on using adsorption for liquid fuel desulfurization. Commercially available sorbents (i.e., zeolites, activated carbon and activated alumina) were used in all of these studies. Weitkamp et al. reported that thiophene adsorbed more selectively than benzene on ZSM-5 zeolite. See Weitkamp, J.; Schwark, M.; Ernest, S. "Removal of Thiophene Impurities from Benzene by Selective Adsorption in Zeolite ZSM-5," *J. Chem. Soc. Chem. Commun.* (1991), 1133. Without being bound to any theory, it is believed that this is because thiophene ( $C_4H_4S$ , also known as thiofuran) has a higher dipole moment (0.55 debye) than benzene (non-polar), although their polarizabilities are similar. Based on this study, King et al. studied selective adsorption of thiophene, methyl- and dimethyl-thiophenes (all with one ring) over toluene and p-xylene, also using ZSM-5. See King, D. L.; Faz, C.; Flynn, T. "Desulfurization of Gasoline Feedstocks for Application in Fuel Reforming," *SAE Paper 2000-01-0002*, Soc. Automotive Engineers, Detroit (2000). They showed that thiophene was more selectively adsorbed, both based on fixed bed breakthrough experiments. However, the capacities for thiophene were unfortunately quite low (1-2% wt. adsorbed at 1% thiophene concentration). Both vapor phase and liquid phase breakthrough experiments were done in these studies, and the results from two phases were consistent.

The pore dimensions of ZSM-5 are 5.2-5.6 Å. Hence, organic sulfur compounds with more than one ring will be sterically hindered or excluded. Zeolites with larger pores, as well as larger pore volumes, would appear to be more desirable than ZSM-5 as the selective sorbents. Indeed, results of Salem and Hamid indicated that 13X zeolite as well as activated carbon had much higher sorption capacities for sulfur compounds. See Salem, A. S. H.; Hamid, H. S. "Removal of Sulfur Compounds from Naphtha Solutions Using Solid Adsorbents," *Chem. Eng. Tech.* (1997), 20, 342. Based on the data of Salem and Hamid, *Id.*, the capacity for sulfur compounds by 13X zeolite was approximately an order of magnitude higher than that of ZSM-5, when compared with the data of King et al. (cited above) extrapolated to the same conditions.

Activated alumina (Alcoa Selexsorb) has been used in an adsorption process.

No direct comparison has been made among these commercial sorbents. Their experiments were mostly done in fixed bed adsorbers, by measuring the  
5 breakthrough capacities. Based on the literature, the large pore zeolites (NaX or NaY) are about the same as activated carbon and alumina, in terms of adsorption of thiophene.

As mentioned hereinabove, current sulfur levels found in commercial liquid fuels are commonly obtained by Hydrodesulfurization (HDS) treatment. The HDS method is very effective in removing thiols and sulfides, but it is generally not adequate for the  
10 removal of thiophenic compounds. For instance, the  $\text{H}_2\text{S}$  produced during reaction of some thiophene derivatives is one of the main inhibitors for deep HDS of unreactive species. Ma, X.; Sakanishi, K.; Mochida, I. Hydrodesulfurization Reactivities of Various Sulfur Compounds in Diesel Fuel. *Ind. Eng. Chem. Res.* (1994), 33, 218 and Knudsen, K.G.; Cooper, B.H.; Topsøe, H. Catalyst and Process Technologies for Ultra Low Sulfur-  
15 Diesel. *Appl. Catal. A-Gen.* (1999), 189, 205. For HDS to meet the new federal government mandates, it is believed that reactors with volumes 5-15 times larger (depending on the  $\text{H}_2$  pressure) than those currently used may be needed.

Ma et al. studied fixed-bed adsorption of thiophene compounds from jet fuels and diesel using an undisclosed transition metal compound (5 wt% loading) supported in  
20 silica gel. Ma, X.; Sun, L.; Song, C. A New Approach to Deep Desulfurization of Gasoline, Diesel Fuel and Jet Fuel by Selective Adsorption for Ultra-Clean Fuels and for Fuel Cell Applications. *Catal. Today* (2002), 77, 107 and Ma, X.; Sprague, M.; Sun, L.; Song, C. Deep Desulfurization of Liquid Hydrocarbons by Selective Adsorption for Fuel Cell Applications. *Am. Chem. Soc. Div. Pet. Chem. Prepr.* (2002), 47, 48. For jet fuel,  
25 they obtained a saturation adsorption capacity of 0.015 g of sulfur per  $\text{cm}^3$  of adsorbent and also showed that breakthrough occurs at about 20  $\text{cm}^3$  effluent volume for about 3.2  $\text{cm}^3$  of the metal loaded silica gel. For a model diesel fuel, Ma et al. obtained a breakthrough capacity of 1  $\text{cm}^3$  per gram of adsorbent. The latter was done for removal of dibenzothiophene and 4,6-dibenzothiophene molecules. Collins et al. also performed fixed-  
30 bed adsorption experiments for sulfur removal, but after oxidation of the thiophenic compounds. Collins, F.M.; Lucy, A.R.; Sharp, C. Oxidative Desulphurisation of Oils via Hydrogen Peroxide and Heteropolyanion Catalysis. *J. Mol. Catal. A-Chem.* (1997), 117, 397. Oxidation was accomplished by using hydrogen peroxide, an acid catalyst and a phase transfer agent. Afterwards, the oxidized sulfurs were removed from the diesel oil  
35 using a silica gel. A breakthrough capacity of about 11  $\text{cm}^3$  per gram of silica gel was obtained in this case. Another adsorbent that has been studied was ALCOA Selexsorb, which is an activated alumina. In one specific application (Irvine, R.L. Process for

Desulfurizing Gasoline and Hydrocarbon Feedstocks. U.S. Patent 5,730,860, 1998) this proprietary material was used in a temperature swing adsorption (TSA) process in order to continuously adsorb heteroatoms from hydrocarbon mixtures and produce full boiling range FCC gasoline products with a maximum sulfur content of 30 ppmw.

5           Essentially all industrial adsorption processes are based on van der Waals interactions between the sorbate and the sorbent. Chemical bonds have yet to be exploited. Further, the drawbacks concomitant with HDS appear to render it an inappropriate solution.

10           Thus, it would be desirable to provide an adsorption process for selectively removing sulfur compounds from liquid fuels at ambient conditions, thereby advantageously leading to a major advance in petroleum refining. It would further be desirable to provide highly selective sorbents for this process, thereby overcoming the drawbacks of current commercial sorbents, which are not desirable for this application. Still further, it would be desirable to provide an adsorption process for selectively  
15           removing aromatic compounds from a mixture of aromatic and aliphatic compounds.

### SUMMARY OF THE INVENTION

20           The present invention addresses and solves the above-mentioned drawbacks, and substantially meets the desiderata and advantages enumerated above, by providing a process for removing thiophene and thiophene compounds from liquid fuel. The method comprises the step of contacting the liquid fuel with an adsorbent which preferentially adsorbs the thiophene and thiophene compounds, at a selected temperature and pressure, thereby producing a non-adsorbed component and a thiophene/thiophene compound-rich adsorbed component. The adsorbent comprises any ion-exchanged zeolite, but in a  
25           preferred embodiment, the zeolite is selected from the group consisting of zeolite X, zeolite Y, zeolite LSX, MCM-41 zeolites, silicoaluminophosphates (SAPOs), and mixtures thereof. The zeolite has exchangeable cationic sites, and at least some of the sites have d-block transition metal cation present. The preferential adsorption occurs by  $\pi$ -complexation.

30           In a further embodiment, the invention comprises a process for removing thiophene and thiophene compounds from liquid fuel. The method comprises the step of contacting the liquid fuel with an adsorbent which preferentially adsorbs the thiophene and thiophene compounds, at a selected temperature and pressure, thereby producing a non-adsorbed component and a thiophene/thiophene compound-rich adsorbed component. The  
35           adsorbent may comprise a carrier having a surface area, the carrier having a metal compound dispersed on at least some of the surface area. The metal compound releasably retains the thiophenes. The carrier comprises a plurality of pores having a pore size greater

than the effective molecular diameter of the thiophene/thiophene compounds. The method may further comprise the step of changing at least one of the pressure and temperature to thereby release the thiophene/thiophene compound-rich component from the adsorbent.

In a further embodiment, the invention comprises a process for selective removal of aromatics from hydrocarbons.

### BRIEF DESCRIPTION OF THE DRAWINGS

Objects, features and advantages of the present invention will become apparent by reference to the following detailed description and drawings, in which:

Fig. 1 is a graph depicting equilibrium isotherms of benzene and thiophene on NaY (Si/Al = 2.43) at 120°C; with the lines being fittings by Langmuir-Freundlich isotherm equation;

Fig. 2 is a graph depicting equilibrium isotherms on AgY (56 Ag<sup>+</sup>/unit cell) and CuY (14 Cu<sup>+</sup>/unit cell) at 120°C;

Fig. 3 is a graph depicting thiophene/benzene and thiophene/n-octane breakthrough in AgY, NaY zeolite at room temperature (RT);

Fig. 4 is a graph depicting cumulative pore volumes of sorbents used in Experiment C;

Fig. 5 is a graph depicting pure component equilibrium isotherms of benzene and thiophene on Na-Y (Si/Al=2.43) at 120°C and 180°C; curves are fitted with Dubinin-Astakhov (solid line) and Langmuir-Freundlich (dotted line) isotherms;

Fig. 6 is a graph depicting pure component equilibrium isotherms of benzene and thiophene on Ag-Y (Si/Al=2.43) at 120°C and 180°C; curves are fitted with Dubinin-Astakhov (solid line) and Langmuir-Freundlich (dotted line) isotherms; fitted curves are not shown for benzene adsorption at 180°C because the artificial crossovers to the curves for thiophene at 180°C are observed;

Fig. 7 is a graph depicting pure component equilibrium isotherms of benzene and thiophene on Cu-Y (Si/Al=2.43) at 90°C and 120°C; curves are fitted with Dubinin-Astakhov (solid line) and Langmuir-Freundlich (dotted line) isotherms;

Fig. 8 is a graph depicting pure component equilibrium isotherms of thiophene on Ag-X (Si/Al=1.25) and Ag-Y (Si/Al=2.43) at 120°C;

Fig. 9 is a graph depicting pure component equilibrium isotherms of benzene and thiophene on H-USY (Si/Al=195) at 90°C and 120°C; curves are fitted with Dubinin-Astakhov (solid line) and Langmuir-Freundlich (dotted line) isotherms;

Fig. 10 is a graph depicting pure component equilibrium isotherms of benzene and thiophene on Na-ZSM-5 (Si/Al=10) at 90°C and 120°C; curves are fitted with Dubinin-Astakhov (solid line) and Langmuir-Freundlich (dotted line) isotherms;

Fig. 11 is a graph depicting pure component equilibrium isotherms of benzene and thiophene on activated carbon (Type PCB) at 90°C and 120°C; curves are fitted with Dubinin-Astakhov (solid line) and Langmuir-Freundlich (dotted line) isotherms;

5 Fig. 12 is a graph depicting pure component equilibrium isotherms of benzene and thiophene on modified activated alumina (Selexsorb CDX) at 90°C and 120°C; curves are fitted with Dubinin-Astakhov (solid line) and Langmuir-Freundlich (dotted line) isotherms;

10 Fig. 13 is a graph comparing equilibrium adsorption isotherms of thiophene at 120°C;

Figs. 14-21 are graphs depicting various breakthrough curves;

Fig. 22 is a graph depicting pure component equilibrium isotherms for benzene and cyclohexane adsorption on H-USY at 120°C and 180°C; curves are fitted with Dubinin-Astakhov (solid lines) and Langmuir-Freundlich (dotted lines) isotherms;

15 Fig. 23 is a graph depicting pure component equilibrium isotherms for benzene and cyclohexane adsorption on Na-Y at 120°C and 180°C; curves are fitted with Dubinin-Astakhov (solid lines) and Langmuir-Freundlich (dotted lines) isotherms;

20 Fig. 24 is a graph depicting pure component equilibrium isotherms for benzene and cyclohexane adsorption on Ag-Y at 120°C and 180°C; curves are fitted with Dubinin-Astakhov (solid lines) and Langmuir-Freundlich (dotted lines) isotherms;

Fig. 25 is a graph depicting pure component equilibrium isotherms for benzene and cyclohexane adsorption on Pd-Y at 120°C; curves are fitted with Dubinin-Astakhov (solid lines) and Langmuir-Freundlich (dotted lines) isotherms;

25 Fig. 26 is a graph depicting pore size distributions of Na-Y, Ag-Y, Pd-Y and H-USY;

Fig. 27 is a graph comparing experimental and GCMC simulation for adsorption of benzene on Na-Y;

Fig. 28 is a graph comparing experimental and GCMC simulation for adsorption of benzene on H-USY;

30 Fig. 29 is a graph comparing experimental and GCMC simulation for adsorption of benzene on Ag-Y;

Fig. 30 is a graph depicting thiophene breakthrough curve in reduced Cu-Y zeolite at RT ( $C_i = 2000$  ppmw thiophene; solvent: n-octane);

35 Fig. 31 is a graph depicting thiophene breakthrough curve in Ag-Y zeolite at RT ( $C_i = 2000$  ppmw thiophene; solvent: n-octane);

Fig. 32 is a graph depicting thiophene breakthrough curves in reduced Cu-Y zeolite at RT ( $C_i = 500$  ppmw thiophene; solvent: n-octane);

Fig. 33 is a graph depicting GC-FPD chromatogram of commercial unleaded regular gasoline;

Fig. 34 is a graph depicting GC-FPD chromatogram of commercial diesel gasoline;

5 Fig. 35 is a graph depicting breakthrough of total sulfur in a fixed-bed adsorber with Cu(I)-Y or AC/ Cu(I)-Y adsorbents, during gasoline treatment at RT.  $C_i$  is the total sulfur concentration at saturation conditions;

Fig. 36 is a graph depicting progression GC-FPD chromatograms of sulfur compounds during gasoline treatment with Cu(I)-Y. Also shown is processed fuel volume values normalized by weight of adsorbent;

Fig. 37 is a graph depicting breakthrough of thiophene or methyl-thiophene or benzothiophene or methyl-benzothiophene in a fixed-bed adsorber with Cu(I)-Y adsorbent, throughout gasoline treatment at RT.  $C_j$  is the sulfur concentration for each species at saturation conditions;

15 Fig. 38 is a graph depicting progression GC-FPD chromatograms of sulfur compounds during gasoline treatment with AC/ Cu(I)-Y. Also shown is processed fuel volume values normalized by weight of adsorbent;

Fig. 39 is a graph depicting breakthrough of thiophene or methyl-thiophene or benzothiophene or methyl-benzothiophene in a fixed-bed adsorber with AC/ Cu(I)-Y adsorbent, throughout gasoline treatment at RT.  $C_j$  is the sulfur concentration for each species at saturation conditions;

Fig. 40 is a graph depicting breakthrough of total sulfur in a fixed-bed adsorber with AC/ Cu(I)-Y adsorbent, during diesel treatment at RT.  $C_i$  is the total sulfur concentration at saturation conditions;

25 Fig. 41 is a graph depicting progression GC-FPD chromatograms of sulfur compounds during diesel treatment with AC/ Cu(I)-Y. Also shown is processed fuel volume values normalized by weight of adsorbent;

Fig. 42 is a graph depicting breakthrough of dibenzothiophene ( $i$ ) or 4-methyl-dibenzothiophene or 4,6-dimethyl-dibenzothiophene or 3,6-dimethyl-dibenzothiophene in a fixed-bed adsorber with AC/ Cu(I)-Y adsorbent, throughout diesel treatment at RT.  $C_j$  is the sulfur concentration for each species at saturation conditions;

Fig. 43 is a graph depicting FTIR spectra of gasoline or diesel for the C-H stretching region;

Fig. 44 is graph depicting gasoline sulfur breakthrough in CuY zeolite at RT (flow rate = 0.5 ml/min);

Fig. 45 is a graph depicting GC-FPD for desulfurization of gasoline with AC/Cu(I)-Y;



Fig. 46 is a graph depicting GC-FPD for a commercial diesel fuel;

Fig. 47 is a graph depicting breakthrough of total sulfur in a fixed-bed adsorber with Ni(II)-Y (LPIE-RT) or Ni(II)-X (LPIE-RT) adsorbents, for diesel feed at RT.  $C_i$  is the total sulfur concentration at saturation conditions;

5 Fig. 48 is a graph depicting a faujasite zeolite framework with cation sites;

Fig. 49A is a graph depicting breakthrough of benzothiophene or dibenzothiophene or 4-methyl-dibenzothiophene or 4,6-dimethyl-dibenzothiophene or 2,4,6-trimethyldibenzothiophene in a Ni(II)-Y (LPIE-RT) adsorbent, with diesel feed at RT;

10 Fig. 49B is a graph depicting breakthrough of benzothiophene or dibenzothiophene or 4-methyl-dibenzothiophene or 4,6-dimethyl-dibenzothiophene or 2,4,6-trimethyldibenzothiophene in a Ni(II)-X (LPIE-RT) adsorbent, with diesel feed at RT;

15 Fig. 50 is a graph depicting breakthrough of total sulfur in a fixed-bed adsorber with Ce(IV)-Y (LPIE-80) or Ni(II)-Y (LPIE-135) or Ni(II)-Y (SSIE-500) adsorbents, for diesel feed at room temperature.  $C_i$  is the total sulfur concentration at saturation conditions;

20 Fig. 51A is a graph depicting breakthrough of benzothiophene or dibenzothiophene or 4-methyl-dibenzothiophene or 4,6-dimethyl-dibenzothiophene or 2,4,6-trimethyldibenzothiophene in a Ni(II)-Y (SSIE-500) adsorbent, with diesel feed at RT;

25 Fig. 51B is a graph depicting breakthrough of benzothiophene or dibenzothiophene or 4-methyl-dibenzothiophene or 4,6-dimethyl-dibenzothiophene or 2,4,6-trimethyldibenzothiophene in a Ce(IV)-Y (LPIE-80) adsorbent, with diesel feed at RT;

Fig. 52 is a graph depicting breakthrough of total sulfur in a fixed-bed adsorber with Selexsorb CDX/Ni(II)-X (LPIE-RT) or Selexsorb CDX/Ni(II)-Y (SSIE-500) adsorbents, for diesel fuel at RT.  $C_i$  is the total sulfur concentration at saturation conditions;

30 Fig. 53 a graph depicting breakthrough of benzothiophene or dibenzothiophene or 4-methyl-dibenzothiophene or 4,6-dimethyl-dibenzothiophene or 2,4,6-trimethyldibenzothiophene in a Selexsorb CDX/Ni(II)-Y (SSIE-500) adsorbent, with diesel fuel at RT;

35 Fig. 54 is a graph depicting total sulfur content of desulfurized diesel during breakthrough in different Ni(II)-zeolites based on a feed with 297 ppmw-S total sulfur content;

Fig. 55 is a graph depicting total sulfur content of desulfurized diesel during breakthrough in different layered beds based on a feed with 297 ppmw-S total sulfur content;

Fig. 56 is a graph depicting breakthrough of total sulfur in a fixed-bed adsorber with fresh and regenerated Ni(II)-Y (SSIE-500) adsorbents, with diesel feed at RT. The adsorbents were regenerated in air at 350°C; and

Fig. 57 is a graph depicting breakthrough of total sulfur in a fixed-bed adsorber with fresh and regenerated Ce(IV)-Y (LPIE-80) adsorbents, with diesel feed at RT. The adsorbents were regenerated in air at 450°C.

#### DETAILED DESCRIPTION OF THE PREFERRED EMBODIMENTS

The present invention is predicated upon the unexpected and fortuitous discovery that thiophene and thiophene compounds are adsorbed slightly more selectively via  $\pi$ -complexation than is benzene. This is quite counter-intuitive, as it would be expected that benzene, having more double bonds (3) and more  $\pi$  electrons than thiophene (2 double bonds), would be more selectively adsorbed via  $\pi$ -complexation. An example of a compound having more double bonds being more selectively adsorbed than a compound having fewer double bonds may be found in U.S. Patent No. 6,215,037, issued to Padin, Munson and Yang in 2001 and entitled, "Method for Selective Adsorption of Dienes."

Without being bound to any theory, it is believed that this counter-intuitive, slightly higher selectivity for thiophene/thiophene derivatives/compounds may be explained by the following theory. The sulfur atom in the five-member thiophene ring has more electrons than the carbons. As such, the S atom, with its available electrons and relatively strong attraction, may be aiding in the  $\pi$ -complexation bonding, thus contributing to the higher selectivity of the present sorbents for thiophenes over benzene. How much the sulfur could contribute to  $\pi$ -complexation bonding, however, is not predictable.

The present invention is a startling and useful discovery, in that the sorbents and process of the present invention adsorb more than 1 mmol/gram of thiophene at  $10^{-5}$  atm. The present inventive method utilizing sorbents which adsorb via  $\pi$ -complexation may be used to remove sulfur compounds (for example, heterocyclic diunsaturated sulfur compounds, including but not limited to thiophene, thiophenic compounds, and/or derivatives thereof) from hydrocarbons such as liquid fuels (including, but not limited to gasoline, diesel fuels, coal and shale derived liquid fuels, methanol, and the like). Liquid fuels have a high concentration of aromatics, such as, e.g., benzene, and a low concentration of thiophene and thiophene compounds (in the parts-per-million (ppm)).

Thus, it is one important aspect of the present invention that the inventive process adsorbs the thiophenes at least slightly more selectively than benzene.

This is a substantial advance over currently available commercial sorbents, which adsorb little, if any, thiophene or thiophene compounds at low concentrations. For example, activated carbon was recently tested by the present inventors, and was found to  
5 behave similarly to Na-Y (discussed in further detail below), in that it adsorbed very little (below 1/10 mmol/gram) benzene and thiophene at  $10^{-5}$  atm.

Without being bound to any theory, it is believed that the higher sorbent capacity of embodiments of the present invention may be due to a sorbent pretreatment  
10 method of an embodiment of the present invention wherein the sorbent is activated at a temperature ranging between about 250°C and about 600°C, and is then cooled. In an embodiment, the activation may be carried out for an amount of time ranging between about zero hours and about 20 or more hours. In an alternate embodiment, the activation may be carried out for an amount of time ranging between about 5 hours and about 15  
15 hours. In a further embodiment, the activation may be carried out for an amount of time ranging between about 6 hours and about 12 hours. In an embodiment, the pretreatment process may take place in an inert, air, dry air, and/or reducing atmosphere, depending on the metal or metal cation used. Non-limitative examples thereof include the following: when the metal cation is  $\text{Ni}^{2+}$ , pretreating (activating and/or cooling) may take place in an  
20 inert atmosphere, in air, and/or in a dry air atmosphere. When the metal cation is  $\text{Cu}^{+}$ , activation may take place in an inert atmosphere and/or in a reducing atmosphere, and cooling may take place in an inert atmosphere. Some non-limitative examples of the reducing atmosphere include reducing gases, such as, for example, hydrogen and/or carbon monoxide, and/or any other suitable reducing gas.

Further, the adsorbents contemplated by the present invention may be  
25 regenerated after use by any suitable method. In an embodiment, the regenerating may be accomplished by calcining the adsorbent. The calcining may be carried out for any suitable length of time and at any suitable temperature sufficient to substantially remove the thiophene/thiophene compounds from the adsorbent. In an embodiment, the calcining  
30 may be carried out for an amount of time ranging between about zero hours and about 20 or more hours. In an alternate embodiment, the calcining may be carried out for an amount of time ranging between about 5 hours and about 15 hours. In an embodiment, the calcining may be carried out at a temperature ranging between about 300°C and about 600°C. The present inventors found satisfactory desulfurization results using sorbents that  
35 had been calcined between about 6 hours and about 12 hours at a temperature ranging between about 350°C and 450°C. The sorbents of the present invention, one example of which is Cu(I)Y, may be substantially fully regenerated by first calcining/air (and/or

oxygen) oxidation (e.g., at about 350°C), followed by auto-reduction in an inert atmosphere (e.g., at about 450°C). Another non-limitative example is Ni(II)Y, which may be substantially fully regenerated by calcination in dry air (e.g., at about 350°C) for about 6 hours. Generally, the stability of the Ni(II) ion allows for its regeneration without the use of further activation steps. As a result, the Ni(II)Y zeolites may in some instances be more commercially advantageous than other sorbents.

The present inventive process may advantageously be run at ambient temperature and pressure, which is highly desirable for a variety of reasons. It is much less energy consuming to run processes at ambient temperature and pressure. Further, conventional catalytic desulfurizing processes are typically run at high temperatures, e.g., 700°C, and high pressures, causing the (very expensive) catalyst to be continually deactivated. Further, the reactor size of a conventional process would need to be exponentially increased over present reactor sizes in order to remove thiophenes lower than the currently acceptable several hundred ppm. Still further, the present inventive process may be used as a first line desulfurizing process, and/or as a clean up desulfurizing process to remove sulfur compounds missed by conventional processes, such as those processes discussed above (e.g., HDS). It could be very useful to have the option to add the present invention as a downstream "clean up" desulfurizing process, in that it may not be necessary to revamp current refining processes upstream from the present inventive process. This could solve the cost-prohibitive problems encountered by some refiners.

Without being bound to any theory, it is also believed that the excellent desulfurization (of fuels such as, for example, gasoline and diesel) results as discussed hereinbelow in embodiments of the present invention may at least in part be due to the addition of a relatively thin layer of another sorbent as a guard bed. It is contemplated that all suitable commercial sorbents may be used as a guard bed. In one non-limitative embodiment(s) discussed herein, the present inventors included a guard bed as about 25% of the bed at the inlet thereto; while the main bed that was doing the purification work remained an ion-exchanged zeolite (suitable examples of which are discussed herein). This sorbent proved orders of magnitude more effective than known sorbent(s).

The process and sorbents of the present invention may have quite significant cost benefits on the future energy picture. For example, for a full tank of gas, it is estimated that it would cost about 70 cents to remove the sulfur from the current 350 ppm to below 5 ppm. If some blending were done, to meet the new (2006) EPA standard, then it is estimated that it would cost about 12 cents. These costs are based on the assumption that the sorbent is disposable - no regeneration. However, it is estimated that the cost could be considerably less if the sorbent were regenerated (for example, as described

above, i.e., calcination alone or air oxidation followed by auto-reduction in inert atmosphere).

Although the process of the present invention has specifically tested Ni-Y, Cu-Y and Ag-Y (as well as other sorbents), it is to be understood that Type X zeolites may in some cases be as good as, or better zeolites than Y zeolites, since more cations are available in X zeolites. Further, it is to be understood that other zeolites are contemplated as being within the scope of the present invention. Still further, it is to be understood that any metal and/or ion that will form  $\pi$ -complexation bonds with thiophene and thiophene compounds may be used. Various metals and/or their ions (including, but not limited to d-block transition metals) may be used in place of the nickel, copper, or silver, as it is believed that these metals will form  $\pi$ -complexation bonds with thiophene and thiophene compounds. In particular, it is believed that  $\text{Mn}^{2+}$ ,  $\text{Fe}^{2+}$ ,  $\text{Co}^{2+}$ ,  $\text{Cd}^{2+}$ ,  $\text{Zn}^{2+}$ ,  $\text{Ga}^{3+}$ , and  $\text{Pd}^0$  would be as effective as  $\text{Ni}^{2+}$ ,  $\text{Cu}^+$ , and  $\text{Ag}^+$ . Further, the metals do not need to be ion-exchanged, but rather may be dispersed (monolayer dispersion, island dispersion, etc.) on a carrier (such as, for example, silica, alumina, etc.) by any suitable method.

The present inventors noted that chemical complexation adsorbents, such as those for  $\pi$ -complexation, have barely been utilized in industrial adsorption applications. The  $\pi$ -complexation bonds are stronger than those formed by van der Waals interactions, but they are also weak enough as to be broken by traditional engineering means such as increasing temperature and/or decreasing pressure. Therefore, the present inventors have fortuitously tailored and developed new adsorbents for processes where selective adsorption is needed, such as in the case of sulfur removal from fuels. The present inventors have also fortuitously discovered that nickel, copper and silver exchanged zeolites, Ni(II)-Y, Ag-Y and Cu(I)-Y are excellent adsorbents for removal of thiophene molecules from liquid hydrocarbon mixtures. Breakthrough and saturation adsorption capacities obtained for an influent concentration of 760 ppmw sulfur (or 2000 ppmw thiophene) in *n*-octane followed the order Cu(I)-Y > Ag-Y > H-Y > Na-Y and Cu(I)-Y > H-Y > Na-Y > Ag-Y, respectively. For the case of 190 ppmw sulfur in mixtures containing both benzene and *n*-octane, Cu(I)-Y adsorbed 0.70 and 1.40 wt% sulfur at breakthrough and saturation, respectively.

In general, the nickel adsorbents tested followed this order for total sulfur adsorption capacity at breakthrough: Selexsorb CDX (alumina)/Ni(II)-Y (SSIE-500) > Selexsorb CDX (alumina)/Ni(II)-X (LPIE-RT) > Ni(II)-Y (SSIE-500) > Ni(II)-X (LPIE-RT) > Ni(II)-Y (LPIE-135).

In embodiments of the present invention,  $\pi$ -complexation adsorbents are used, such as, for example, to remove sulfur compounds from commercial fuels, in particular gasoline and diesel, at RT and atmospheric pressure using fixed-bed

adsorption/breakthrough techniques together with GC-FPD (Flame Photometric Detector) and FTIR analysis.

In an embodiment of the present invention, the process for removing thiophene and thiophene compounds from liquid fuel comprises the step of contacting the liquid fuel with an adsorbent which preferentially adsorbs the thiophene and thiophene compounds, at a selected temperature and pressure, thereby producing a non-adsorbed component and a thiophene/thiophene compound-rich adsorbed component. It is to be understood that in the "thiophene/thiophene compound-rich adsorbed component" term as used herein, the thiophenes may not be the greatest amount of adsorbate. For example, in the case of liquid fuels having a very high concentration of aromatics, and a very low concentration of thiophenes, the adsorbed phase will actually contain more benzene than thiophene, because there is much more benzene than thiophene in the solution. The adsorbed phase may have thiophene/benzene at a ratio of about 1/2. However, that would be enough to advantageously purify the solution.

The adsorbent comprises any ion-exchanged zeolite, but in a preferred embodiment, the zeolite is selected from the group consisting of zeolite X, zeolite Y, zeolite LSX, MCM-41 zeolites, silicoaluminophosphates (SAPOs), and mixtures thereof. The zeolite has exchangeable cationic sites, and at least some of the sites have metal cation present. The preferential adsorption occurs by  $\pi$ -complexation.

In a further embodiment of the process described above, the adsorbent may alternately include a carrier having a surface area, the carrier having a metal compound (a non-limitative example of which is a d-block transition metal) dispersed on at least some of the surface area. Further, the metal compound releasably retains the thiophenes. The carrier comprises a plurality of pores having a pore size greater than the effective molecular diameter of the thiophene/thiophene compounds. The method may further comprise the step of changing at least one of the pressure and temperature to thereby release the thiophene/thiophene compound-rich component from the adsorbent.

Chemical complexation bonds are generally stronger than van der Waals interactions (thus giving rise to higher selectivities), yet weak enough to be reversible (i.e., to be broken by simple engineering means). Therefore, a tremendous opportunity exists for developing new sorbents (and new applications in separation and purification) by using weak chemical bonds, including various forms of complexation bonds. For purification, vapor phase results can be applied directly to liquid phase applications. In the present invention, the inventors have used molecular orbital calculations to obtain a basic understanding for the bonding between the sorbates and sorbent surfaces, and further, to develop a methodology for predicting and designing  $\pi$ -complexation sorbents for targeted molecules (see, for example, Huang, H. Y.; Padin, J.; Yang, R. T. "*Ab Initio* Effective Core

Potential Study of Olefin/Paraffin Separation by Adsorption via  $\pi$ -Complexation: Anion and Cation Effects on Selective Olefin Adsorption," *J. Phys. Chem. B.* (1999), 103, 3206; and Huang, H. Y.; Padin, J.; Yang, R. T. "Comparison of  $\pi$ -Complexations of Ethylene and Carbon Monoxide and  $\text{Cu}^+$  and  $\text{Ag}^+$ ," *Ind. Eng. Chem. Res.* (1998), 38, 2720).

5 In the present invention, the inventors obtained first results on new sorbents for desulfurization using  $\pi$ -complexation.  $\text{Cu(I)Y}$ ,  $\text{AgY}$ ,  $\text{Ni(II)Y}$  were some of the sorbents, and thiophene and benzene were used as the model system. Since  $\text{NaX}$  (i.e., 13X) or  $\text{NaY}$  is among the best commercially available sorbents for thiophene,  $\text{NaY}$  was used as the reference for comparison.

10 The sulfur breakthrough curves with  $\text{AgY}$  and  $\text{NaY}$  zeolites (Fig. 3), with a liquid feed of thiophene in octane, shows  $\text{AgY}$  to be an excellent sorbent.

Further experiments were run with  $\text{Cu(I)Y}$ . Surprisingly, even though the results with  $\text{AgY}$  were very good, the results with  $\text{Cu(I)Y}$  were better than those of  $\text{AgY}$ . The sorbent capacity of  $\text{Cu(I)Y}$  is much higher than that of  $\text{AgY}$ , and very pure octane was  
15 obtained for extended periods of time. The sulfur capacity of  $\text{Cu(I)Y}$  zeolite was found to be about 2.55 mmol/g (or, 21.4 wt %). This is an extremely high capacity because the experiments were removing ppm levels of sulfur.  $\text{Cu(I)-Y}$  (auto-reduced  $\text{Cu(II)-Y}$ ) zeolites were used to separate low concentration sulfur molecules from commercial gasoline and diesel samples, at room temperature and atmospheric pressure. Substantially  
20 sulfur-free fuels were obtained with  $\text{Cu(I)-Y}$  and a combination of activated carbon (AC) and  $\text{Cu(I)-Y}$ . Activated carbon was used as a guard bed. Breakthrough and saturation adsorption capacities obtained for an influent average total concentration of 335 ppmw sulfur in gasoline showed that  $\text{Cu(I)-Y}$  is capable of processing about 14.7  $\text{cm}^3$  of substantially sulfur-free gasoline per gram of adsorbent and removing about 1.4 wt%  
25 sulfur at saturation. When using activated carbon as a guard bed with  $\text{Cu(I)-Y}$  zeolite, the combination is capable of processing about 19.6  $\text{cm}^3$  of substantially sulfur-free gasoline per gram of adsorbent. In the case of diesel fuel, AC/ $\text{Cu(I)-Y}$  adsorbed about 1.08wt% and 1.85 wt% total sulfur at breakthrough and saturation, respectively. At breakthrough, the adsorbent plus guard bed is capable of processing about 34.3  $\text{cm}^3$  of substantially sulfur-free diesel per gram of adsorbent. GC-FPD data reveals the  $\pi$ -complexation adsorbents are capable of removing heavily substituted thiophenes, benzothiophenes, and dibenzothiophenes, which is not possible using conventional HDS reactors.

Solid state ion exchanged (SSIE)  $\text{Ni(II)-Y}$ , with alumina acting as a guard-bed, processes 19  $\text{cm}^3$ /g of diesel with an average sulfur content of 0.220 ppmw.

35  $\text{Ag}$ -exchanged faujasite was claimed for thiophene removal in U.S. Patent No. 4,188,285 issued to Michlmayr. In sharp contrast to the present invention, the '285 preferred temperature for adsorption was 200-350°C, and the sorbent was not dehydrated

by heat-treatment prior to adsorption. Also in sharp contrast to the present invention, the '285 sulfur capacities were very low, at about 0.07-0.15 wt% for Ag-Y. In the '285 patent, the highest sulfur capacity (of 0.2 wt%) was obtained with the lowest Ag content, with USY zeolite. The '285 sorbent was apparently intended for bonding the sulfur atom with Ag. It was not intended for  $\pi$ -complexation. In contrast, the sorbents of the present invention, for example, the Cu(I)Y sorbent has a sulfur capacity > 100 times larger.

Vansant et al. in European Patent Publication No. 0 275 855 investigated Cu(II)Y for thiophene removal. In contrast to the present invention, the '855 Cu<sup>2+</sup> exchanged Y zeolite was purposely heat-treated in air (to 200-550°C) to maintain the Cu<sup>2+</sup> in the divalent state. Thus, in contrast to the present invention, in the '855 publication adsorption by  $\pi$ -complexation was not intended. The '855 publication discloses low thiophene capacities (the highest was 1.6 wt%). In sharp contrast, the thiophene capacities of the present invention were about 21.4 wt%.

Figs. 14-21 are graphs depicting various breakthrough curves.

To further illustrate the present invention, the following examples are given. It is to be understood that these examples are provided for illustrative purposes and are not to be construed as limiting the scope of the present invention.

## EXAMPLES

### EXPERIMENT A

**Sorbent Preparation.** Cu<sup>+</sup>-Y was prepared by ion exchange of Na-Y zeolites (Si/Al=2.43, 56 Al atoms/u.c., Strem Chemical) with Cu(NO<sub>3</sub>)<sub>2</sub> followed by reduction of Cu<sup>2+</sup> to Cu<sup>+</sup>, since Cu(I) is not soluble in water. First, as-received Na-Y was exchanged twice using excess amounts (10-fold cation-exchange-capacity (CEC) assuming that one Cu<sup>2+</sup> compensates two aluminum sites) of 0.5 M Cu(NO<sub>3</sub>)<sub>2</sub> at RT for 24 hours. After the exchange, the zeolite suspension was filtered and washed with copious amount of de-ionized water. The product was dried at 100°C overnight. In this study, reduction of Cu<sup>2+</sup> to Cu<sup>+</sup> was carried out in He at 450°C for 1 hour. Ag<sup>+</sup> ion-exchanged Y-zeolite (Ag-Y) was prepared at RT for 24 hours in the same manner as Cu<sup>2+</sup> exchange, using 5-fold excess AgNO<sub>3</sub> (0.1M).

Single component isotherms for benzene and thiophene were measured at 120°C using standard gravimetric methods. A Shimadzu TGA-50 automatic recording microbalance was employed. Helium (Pre-purified grade, Metro welding, 99.995%) was used as the carrier gas and was first passed through two consecutive gas-wash bottles (to ensure saturation), which contained benzene (HPLC grade, Aldrich, 99.9+%) or thiophene (Aldrich, 99+%). After diluting the concentration to the desired value by blending with additional helium, the mixture was directed into the microbalance.



**Molecular Orbital Computational Details.** Molecular orbital (MO) studies on the  $\pi$ -complexation bonding for benzene and sorbent surfaces had been investigated recently.

See Takahashi, A.; Yang, F. H.; Yang, R. T. "Aromatics/Aliphatics Separation by

5 Adsorption: New Sorbents for Selective Aromatics Adsorption by  $\pi$ -Complexation," *Ind. Eng. Chem. Res.* (2000), 39, 3856. In this work, similar MO studies were extended to thiophene and sorbent surfaces. The Gaussian 94 Program in Cerius2 molecular modeling software from Molecular Simulation, Inc. was used for all calculations. MO calculations for thiophene and sorbent surfaces were performed at the Hartree-Fock (HF) and density  
10 functional theory (DFT) level using effective core potentials (ECPs).

The LanL2DZ basis set is a double- $\zeta$  basis set containing ECP representations of electrons near the nuclei for post-third-row atoms. The reliability of this basis set has been confirmed by the accuracy of calculation results as compared with experimental data. Therefore, the LanL2DZ basis set was employed for both geometry  
15 optimization and natural bond orbital (NBO) analysis.

The restricted Hartree-Fock (RHF) theory at the LanL2DZ level basis set was used to determine the geometries and the bonding energies of thiophene on AgCl and CuCl. The simplest models with a single metal chloride interacting with a thiophene molecule were chosen for  $\pi$ -complexation studies. The optimized structures were then  
20 used for bond energy calculations according to the following expression:

$$E_{\text{ads}} = E_{\text{adsorbate}} + E_{\text{adsorbent}} - E_{\text{adsorbent-adsorbate}} \quad (1)$$

where  $E_{\text{adsorbate}}$  is the total energy of thiophene,  $E_{\text{adsorbent}}$  is the total energy of the bare  
25 adsorbent, i.e., the metal chloride, and  $E_{\text{adsorbent-adsorbate}}$  is the total energy of the adsorbate/adsorbent system. A higher value of  $E_{\text{ads}}$  corresponds to a stronger adsorption.

**Natural Bond Orbital (NBO).** The optimized structures were also used for NBO analysis at the B3LYP/LanL2DZ level. The B3LYP approach is one of the most useful self-  
30 consistent hybrid (SCH) approaches, it is Beck's 3-parameter nonlocal exchange functional with nonlocal correlation functional of Lee, Yang and Parr.

The NBO analysis performs population analysis that pertains to localized wave-function properties. It gives a better description of the electron distribution in compounds of high ionic character, such as those containing metal atoms. It is known to  
35 be sensitive for calculating localized weak interactions, such as charge transfer, hydrogen bonding and weak chemisorption. Therefore, the NBO program was used for studying the electron density distribution of the adsorption system.

**Results and Discussion.** Figure 1 shows the equilibrium isotherms of benzene and thiophene on NaY at 120°C. NaY does not have a selectivity for thiophene; however, it adsorbs both benzene and thiophene quite strongly, as evidenced by the still measurable amounts adsorbed at partial pressures as low as 10-100 ppm of 1 atm. As expected, a fixed-bed adsorber experiment using NaY would yield a breakthrough curve. The data were fitted by the Langmuir-Freundlich isotherm, as shown by the lines in the figure.

Figure 2 shows the isotherms of benzene and thiophene on AgY and CuY. Note that: (a) compared with NaY, AgY and CuY adsorb both thiophene and benzene more strongly at below  $10^{-3}$  atm, due to  $\pi$ -complexation; and (b) on a per-cation basis, Cu<sup>+</sup> shows stronger interactions than Ag<sup>+</sup>. Compared with Figure 1, these sorbents adsorbed significantly more thiophene and benzene than NaY at pressures below  $10^{-3}$  atm, and nearly the same amounts at high partial pressures. This result was a clear indication of  $\pi$ -complexation with Ag<sup>+</sup> and Cu<sup>+</sup>; Na<sup>+</sup> could not form  $\pi$ -complexation bonds.

The neutron activation analyses of the sorbent samples showed that the Ag<sup>+</sup> exchange was 100% but the Cu<sup>+</sup> exchange was 23%. On a per-cation basis, the  $\pi$ -complexation with Cu<sup>+</sup> was stronger than that with Ag<sup>+</sup>. This was indeed confirmed by our molecular orbital calculations, as will be discussed. To understand the relative strengths of  $\pi$ -complexation between Ag<sup>+</sup> and Cu<sup>+</sup>, the thiophene adsorption amounts at  $2 \times 10^{-5}$  atm were normalized by Ag<sup>+</sup> or Cu<sup>+</sup> content, and the results are shown in Table 1. It is seen that Cu<sup>+</sup> could adsorb higher thiophene adsorption amounts per cation. In fact, 0.92 thiophene molecule per Cu<sup>+</sup> was obtained at  $2 \times 10^{-5}$  atm at 120°C. This amount was due to Cu<sup>+</sup> since the amount adsorbed by NaY at the same pressure was negligible. At the same pressure, 0.42 thiophene/Ag<sup>+</sup> was obtained. This result indicated strong  $\pi$ -complexation bonds between both Cu<sup>+</sup> and Ag<sup>+</sup>, and that the bond with Cu<sup>+</sup> was stronger.

**Table 1. Thiophene adsorption amount normalized by cation content (thiophene/cation).**

Adsorbent	Ag-Y	Cu-Y
Cation for $\pi$ -complexation	Ag <sup>+</sup>	Cu <sup>+</sup>
Cation Content in Zeolite (wt%)	38.2	8.29
Amount Adsorbed (thiophene molecule/cation)	0.42	0.92

The heats of adsorption for  $\pi$ -complexation were estimated by taking the values at low loadings, and they were obtained from the temperature dependence of the isotherms at low pressures. These values are given in Table 2.

5 **Table 2. Heats of adsorption (kcal/mol) for  $\pi$ -complexation.**

Zeolite	Thiophene	Benzene
Cu(I)-Y	22.3	21.8
Ag-Y	21.4	20.1

**Bond Energies, Geometries and NBO results.** The energies of adsorption calculated using equations 1 and 2 for thiophene and benzene are summarized in Table 3.

10

**Table 3. Summary of energies of adsorption for thiophene and benzene in kcal/mol.**

MCl	$E_{\text{ads}}(\text{Thiophene})$	$E_{\text{ads}}(\text{Benzene})$
CuCl	13.5	12.4
AgCl	9.0	8.6

The theoretical calculations indicate that the  $\pi$ -complexation strengths follow the order  
 15 CuCl > AgCl and more importantly, thiophene > benzene. This trend is in agreement with the experimental data, in Table 2. Chloride was used as the anion in the theoretical calculations, while zeolite framework was the anion in the experiment. It is known that the anion has a large effect on the  $\pi$ -complexation bonds. In the optimized structures of thiophene-MCl complexes, the distance between the thiophene molecule and Cu ion is  
 20 about 0.3 Å shorter than that of thiophene and Ag ion. The NBO analysis is summarized in Tables 4 and 5. There is some donation of electron charges from the  $\pi$ -orbital of thiophene to the vacant s orbital of metals known as  $\sigma$  donation and, simultaneously, back-donation of electron charges from the d orbitals of metals to  $\pi^*$  orbital of thiophene or  $\pi$  back-donation. The  $\pi$  back-donation appears to be important in all cases. The charge  
 25 transfer results again confirmed the experimental data that the relative strengths of the  $\pi$ -complexation bonds follow the order: thiophene > benzene and  $\text{Cu}^+ > \text{Ag}^+$ . On a per cation basis, more thiophene was adsorbed by  $\text{Cu}^+$  than by  $\text{Ag}^+$ , for example, 0.92 molecule/  $\text{Cu}^+$  versus 0.42 molecule/ $\text{Ag}^+$  at  $2 \times 10^{-5}$  atm and 120°C.

**Table 4. Summary of NBO analysis\* of  $\pi$ -complexation between thiophene and MCl.**

MCl	C→M interaction ( $\sigma$ donation) $q_1$	M→C interaction (d - $\pi^*$ back-donation) $q_2$	Net Change $q_1 + q_2$
CuCl	0.037	-0.022	0.015
AgCl	0.022	-0.014	0.008

\* $q_1$  is the amount of electron population change in valence s orbitals of the metal, and  $q_2$  is the total amount of electron population decrease in valence d orbitals of the metal.

5

**Table 5. Summary of NBO analysis\* of  $\pi$ -complexation between benzene and MCl.**

MCl	C→M interaction ( $\sigma$ donation) $q_1$	M→C interaction (d - $\pi^*$ back-donation) $q_2$	Net Change $q_1 + q_2$
CuCl	0.011	-0.013	0.002
AgCl	0.003	-0.007	0.004

\* $q_1$  is the amount of electron population change in valence s orbitals of the metal, and  $q_2$  is the total amount of electron population decrease in valence d orbitals of the metal.

10

## EXPERIMENT B

**Thiophene Removal Using Sodium and Silver Cation in Faujasite Zeolites.** Work has been done on different adsorbents to remove sulfur from mixtures, such as, for example, thiophene from benzene or n-octane based solutions. These adsorbents include sodium and silver forms of faujasite type zeolites, particularly, Y type zeolites. Initial studies were done for the case of an inlet concentration of 2000 ppmw of thiophene in either benzene or n-octane.

15

**Sorbent Preparation.** Sodium Y Zeolite powder was obtained from Strem Chemicals. Silver Y Zeolite was obtained by ion exchanging NaY at RT. The solution was prepared using a silver nitrate salt and deionized water (~0.2 M). A 4-fold excess amount of silver was used to ensure exchange completion. After ion exchanging for 48 hours, the adsorbent was recovered by filtration and washed with large amounts of deionized water. Drying was performed at RT.

20

25

**Breakthrough Experiments.** Breakthrough experiments were performed in a custom made quartz reactor equipped with a glass frit. The adsorbent was loaded inside the reactor (usually 1 or 2 grams) and activated *in situ* under a helium atmosphere at 350°C for 24 hrs. The adsorbent was then cooled down to RT. At this point, the sorbent was wetted

by pouring down sulfur free solvent (benzene or n-octane) for about 30 minutes. This stream was then changed to one containing 2000 ppmw thiophene. Samples were collected at different time intervals, and the thiophene outlet concentration was analyzed using a GC unit equipped with a polar column at 65°C.

**Preliminary Results.** Figure 3 shows breakthrough curves for thiophene in either benzene or n-octane in sodium or silver forms of Y Zeolite.

*Thiophene adsorption amounts after saturation.*

	NaY	AgY
Solvent	Saturation Amount (mmol/g)	
Benzene	0.102	0.171
n-Octane	----	0.898

Integration of the area above the curves yield the adsorption saturation amounts presented in the table shown above. For the case of thiophene/benzene mixtures, the calculated thiophene adsorption amounts are not that high. Very recent single component vapor phase adsorption experiments have shown that NaY and AgY may adsorb benzene and thiophene in similar quantities. Thus, benzene may compete for many of the adsorption sites, perhaps leaving thiophene with fewer available sites. However, despite the possibility of competitive adsorption, the presence of silver cations results in an increase in some adsorption capacity. For the case of thiophene/n-Octane mixtures, AgY Zeolite shows great selectivity towards thiophene. Without being bound to any theory, it is believed that this indicates that the interaction between the silver cations and the thiophene molecules is higher than that of n-Octane molecules.

### EXPERIMENT C

In this experiment, the known commercial sorbents such as Na-Y, Na-ZSM-5, H-USY, activated carbon and activated alumina (Alcoa Selexsorb) were included, and a direct comparison was made with Cu-Y and Ag-Y which were the sorbents with  $\pi$ -complexation capability. Thiophene and benzene were used as the model system for desulfurization.

**Sorbent preparation.** Various sorbents were investigated in this work. Four as-received sorbents: Na-type Y-zeolite (Na-Y, Si/Al=2.43, 56 Al atoms/unit cell, Strem Chemical), H-type ultra-stable Y-zeolite (H-USY, Si/Al=195, 0.98 Al atoms/u.c., HSZ-390HUA,

TOSOH Corporation), activated carbon (Type PCB, Calgon Carbon Corporation) and modified activated alumina (Selexsorb CDX, Alcoa Industrial Chemical), were used. According to the product datasheets, Selexsorb CDX is formulated for adsorption of sulfur-based molecules, nitrogen-based molecules, and oxygenated hydrocarbon molecules. Na-Y and H-USY were in powder form (binderless). Since activated carbon was in granular form and activated alumina was in pellet form, they were crushed into powder form for evaluation.

Cu<sup>+</sup>-Y and Ag-Y were prepared as in Experiment A, above. 13X (Si/Al=1.25, Linde, lot#945084060002) was used for the preparation of Cu-X (10 fold CEC solution of Cu(NO<sub>3</sub>)<sub>2</sub>, ion-exchanged at 65°C for 24 hrs, three times) and Ag-X (5-fold CEC solution of AgNO<sub>3</sub>, ion-exchanged at RT for 24 hrs, twice). Na-type ZSM-5 (Na-ZSM-5) was prepared at RT by Na<sup>+</sup>-exchange of NH<sub>4</sub>-ZSM-5 (Si/Al=10, SM-24, ALSI-PENTA Zeolite GmbH).

**Isotherm and uptake rate measurements.** The strength of adsorptive interaction between adsorbents and thiophene/benzene was compared. Extremely low partial pressures at less than 10<sup>-5</sup> atm would be necessary to meet this objective if isotherms were measured at ambient temperature, because the isotherms at ambient temperature are fairly flat and are difficult to compare each other. However, it is very difficult to obtain and control such low partial pressures experimentally. Therefore, single component isotherms for benzene and thiophene were measured at 90°C, 120°C and 180°C using standard gravimetric methods. A Shimadzu TGA-50 automatic recording microbalance was employed. Helium (Pre-purified grade, Metro welding, 99.995%) was used as the carrier gas and was first passed through two consecutive gas-wash bottles (to ensure saturation), which contained benzene (HPLC grade, Aldrich, 99.9+%) or thiophene (Aldrich, 99+%). After diluting the concentration to the desired value by blending with additional helium, the mixture was directed into the microbalance.

Isosteric heats of adsorption were calculated using the Clausius-Clapeyron equation from isotherms at different temperatures. Nitrogen isotherms at 77K measured with a Micromeritics ASAP 2010 system were used for pore size distribution and pore volume determination. Pore size distributions were calculated with Horvath-Kawazoe equation. Slit pore model was used for activated carbon, and cylindrical pore model was used for ZSM-5 and activated alumina, while spherical pore model was applied to Y-zeolites and X-zeolites. As for the parameters for H-K equation such as polarizability, magnetic susceptibility, density, etc., default values in Micromeritics ASAP system were used for the calculation of pore sizes. See "Accelerated Surface Area and Porosimetry System Operator's Manual V3.02," Micromeritics Instrument Corp. (1997). The diffusion

time constants,  $D/r^2$  ( $s^{-1}$ ), were calculated from the uptake rates. See Yeh, Y. T, "Diffusion and Adsorption of Gases in Molecular Sieves," Ph.D. Dissertation, University of New York at Buffalo, Buffalo, New York, (1989). In this experiment, short time region (up to 30 % uptake) and spherical adsorbent model were used.

5

**Chemical Analysis.** The compositions of Cu-Y and Ag-Y were characterized using neutron activation analysis (NAA) in the research nuclear reactor of the Phoenix Memorial Laboratory at the University of Michigan. The sample was irradiated sequentially for one minute at a core-face location with an average thermal neutron flux of  $2 \times 10^{12}$  n/cm<sup>2</sup>/s.

10 Two separate gamma-ray spectra were then collected for each sample with a high resolution germanium detector: one after 13-minute decay to determine the concentrations of Al, Ag and Cu, and a second after a 1 hour and 56-minute decay to analyze for Na. Gamma energy lines at 1779 keV, 632.99 keV, 1039.20 keV and 1368.6 keV were used for the determination of Al, Ag, Cu and Na concentration, respectively.

15 Molecular Orbital Computational Details and Natural Bond Orbitals are as described in Experiment A above.

**Models for Ag-Zeolite (AgZ) and Cu-Zeolite (CuZ).** The zeolite models selected for this study are similar to the ones used by Chen and Yang (see Chen, N. and R.T. Yang,

20 "Ab Initio Molecular Orbital Study of Adsorption of Oxygen, Nitrogen, and Ethylene on Silver-Zeolite and Silver Halides," *Ind. Eng. Chem. Res.* (1996), 35, 4020), with the molecular formula of  $(HO)_3Si-O-Al(OH)_3$ , and the cation  $Ag^+$  or  $Cu^+$  sits 2 – 3 Å above the bridging oxygen between Si and Al. This is a good cluster model representing the chemistry of a univalent cation bonded on site II (SII) of the faujasite framework (Z).

25 Once the optimized structures of AgZ and CuZ are obtained at the B3LYP/LanL2DZ level, then a molecule of thiophene ( $C_4H_4S$ ) or benzene ( $C_6H_6$ ) is added onto the cation of the zeolite model, and the resulting structure is further optimized at the B3LYP/LanL2DZ level.

## 30 Results and Discussion

**Characterization of sorbents.** NAA showed that Ag/Al and Na/Al ratios in Ag-Y were 1.13 and 0.01, respectively. This is because  $Ag^+$  is known to have higher selectivity to cation sites in zeolites compared to  $Na^+$ . More than 100% Ag ion-exchange ratio was obtained in Ag-Y, because some Ag ions were located outside the charge-compensating

sites. On the other hand, the Al, Cu, and Na contents in Cu-Y were  $6.10 \pm 0.25$  wt%,  $6.65 \pm 0.05$  wt%, and  $1.50 \pm 0.12$  wt%, respectively. This means that the Cu/Al molar ratio was 0.463, and the Na/Al ratio was 0.289, indicating less selectivity than  $\text{Ag}^+$ . Therefore, Cu ion-exchange for X-zeolite was carried out three times at  $65^\circ\text{C}$  (instead of twice at RT for Cu-Y) for 24 hrs to enhance the ion-exchange.

Figure 4 shows the comparison of the cumulative pore volumes of the sorbents used. Activated carbon has the largest pore volume with small pores, while Na-ZSM-5 has the smallest pore volume. Selexsorb CDX also shows small pores. Because silver is heavier than copper and the silver content in Ag-Y ( $\text{Ag}/\text{Al}=1.13$ ) was more than copper content in Cu-Y ( $\text{Cu}/\text{Al} = 0.463$ ), the density of Ag-Y was higher by 36% ( $\text{Na}_{0.084}\text{Cu}_{0.135}\text{Al}_{0.292}\text{Si}_{0.708}\text{O}_2$ ; MW = 70.27 vs.  $\text{Ag}_{0.330}\text{Al}_{0.292}\text{Si}_{0.708}\text{O}_2$ ; MW = 95.36). Consequently, the pore volume of Ag-Y was about 25 % smaller than that of Cu-Y.

**Benzene/Thiophene adsorption isotherms: Na-Y.** Figure 5 shows the equilibrium isotherms of benzene and thiophene on Na-Y at  $120^\circ\text{C}$  and  $180^\circ\text{C}$ . The data were fitted by the Langmuir-Freundlich and Dubinin-Astakhov isotherms, which are shown by the lines in Figure 5. Barthomeuf and Ha measured benzene adsorption on NaH-Y ( $\text{Si}/\text{Al}=2.43$ , 81%Na) at  $172^\circ\text{C}$ . Their isotherm and calculated heat of adsorption agreed with the data shown in Figure 5 very well, substantially ensuring the accuracy of the isotherms in this work. More benzene was adsorbed on Na-Y than thiophene at pressures lower than  $10^{-2}$  atm. This result indicated that the contribution of the higher polarizability of benzene ( $10.3 \times 10^{-24} \text{ cm}^3$  for benzene vs.  $9.7 \times 10^{-24} \text{ cm}^3$  for thiophene) was larger than the contribution of the dipole moment (0 debye in benzene vs. 0.55 debye in thiophene) and lower magnetic susceptibility ( $9.1 \times 10^{-29} \text{ cm}^3/\text{molecules}$  for benzene vs.  $9.5 \times 10^{-29} \text{ cm}^3/\text{molecules}$  for thiophene). At higher pressures over  $1 \times 10^{-2}$  atm, the benzene adsorption amount became smaller owing to the larger molar volume of benzene than thiophene. Na-Y does not have a selectivity for thiophene; however, it adsorbs both benzene and thiophene quite strongly, as evidenced by the still measurable amounts adsorbed at partial pressures as low as  $10^{-4}$  to  $10^{-3}$  atm.

**Ag-Y and Cu-Y.** Figure 6 and Figure 7 show the isotherms of benzene and thiophene on Ag-Y and Cu-Y. Compared with Figure 5, these sorbents adsorbed significantly more thiophene/benzene than Na-Y at pressures below  $10^{-3}$  atm, and nearly the same amounts at high partial pressures. This result was a clear indication of  $\pi$ -



complexation with  $\text{Ag}^+$  and  $\text{Cu}^+$ ; since  $\text{Na}^+$  could not form  $\pi$ -complexation bonds.

However, the difference in the amounts of thiophene/benzene adsorbed did not reflect the relative strengths of  $\pi$ -complexation between  $\text{Cu}^+$  and  $\text{Ag}^+$  because the  $\text{Cu}^+$  exchange was not complete. The NAA of the sorbent samples showed that the  $\text{Ag}^+$  exchange was 100% but the  $\text{Cu}^+$  exchange was 46%. According to the EPR analysis, about a half of the  $\text{Cu}^{2+}$  was auto-reduced to  $\text{Cu}^+$  after our heat treatment at  $450^\circ\text{C}$  for 1 hr in He. On a per-cation basis, the  $\pi$ -complexation with  $\text{Cu}^+$  was stronger than that with  $\text{Ag}^+$ . This was indeed confirmed by our molecular orbital calculations, as will be discussed. To understand the relative strengths of  $\pi$ -complexation between  $\text{Ag}^+$  and  $\text{Cu}^+$ , the thiophene adsorption amounts at  $2 \times 10^{-5}$  atm were normalized by  $\text{Ag}^+$  or  $\text{Cu}^+$  content, and the results are shown in Table 6. It is seen that  $\text{Cu}^+$  could adsorb higher thiophene adsorption amounts per cation. In fact, 0.92 thiophene molecule per  $\text{Cu}^+$  was obtained at  $2 \times 10^{-5}$  atm at  $120^\circ\text{C}$ . This amount was due to  $\text{Cu}^+$  since the amount adsorbed by NaY at the same pressure was negligible. At the same pressure, 0.42 thiophene/ $\text{Ag}^+$  was obtained. This result indicated strong  $\pi$ -complexation bonds between both  $\text{Cu}^+$  and  $\text{Ag}^+$ , and that the bond with  $\text{Cu}^+$  was stronger.

**Table 6. Thiophene Adsorption Amount Normalized by Cation Content.**  
(thiophene/cation molar ratio)

Adsorbent	Ag-Y	Cu-Y
Cations for $\pi$ -complexation	$\text{Ag}^+$	$\text{Cu}^+$
Cation Content in Zeolite (wt%)	38.2	8.29
Amount Adsorbed (molar ratio)	0.42	0.92

The vapor-phase isotherms of benzene/thiophene on Cu-Y and Ag-Y were not completely reversible within a practical time scale (1 hours to 3 hours), because of relatively strong interaction. However, the bond energies are of the order of 20 kcal/mol, which are weak enough so a substantial fraction of the adsorbed molecules are desorbed in a short period of time. For practical application, thermal desorption or displacement desorption may be a desirable option.

**Cu-X.** In order to increase the  $\text{Cu}^+$  content in the faujasite structure, an X-zeolite ( $\text{Si}/\text{Al} = 1.25$ ) was ion-exchanged with  $\text{Cu}(\text{NO}_3)_2$ . Cu-X was considered to be promising, since larger amounts of  $\text{Cu}^+$  can be present in the structure of zeolite, especially at SIII sites. The color of Cu-X powder after ion-exchange (before auto-reduction) was

more blue than that of Cu-Y, suggesting that more  $\text{Cu}^{2+}$  was contained in X-zeolite than Cu-Y. For faujasite-type zeolites, the cations are designated as SI (the center of hexagonal prism), SI' (opposite SI but located in the cubooctahedron), SII (single six-ring in the supercage), SII' (opposite SII but inside the cubooctahedron), and SIII (near the four-ring windows in the supercage). The cations at SI, SI' and SII' sites are not exposed to the supercage and are shielded by framework oxygen. They cannot interact with molecules inside the supercages directly. SII and SIII sites are exposed to the supercage and can interact with molecules inside the supercage. Because Y-zeolite ( $\text{Si}/\text{Al}=2.43$ ) does not have the SIII cation sites, it is believed that cations at SII site are responsible for the thiophene/benzene adsorption. On the other hand, X-zeolite ( $\text{Si}/\text{Al}=1.25$ ) have a certain amount of SIII sites, based on the results on Ag-X. This additional  $\text{Cu}^+$  located at SIII site should enhance the adsorption amount. However, unfortunately, it was found that Cu-X ( $\text{Si}/\text{Al}=1.25$ ) was not stable at temperatures over  $200^\circ\text{C}$ , and the pore volume was decreased by 60 %. The color of the powder was changed from light blue to dark greenish gray after heating at  $200^\circ\text{C}$  for 1 hour in vacuum. As a result, thiophene adsorption amount on Cu-X after  $450^\circ\text{C}$  auto-reduction was considerably smaller than that on Cu-Y (Isotherms were not shown). To alleviate the destruction of Cu-X structure, the heating rate to  $450^\circ\text{C}$  was reduced to  $0.5^\circ\text{C}/\text{min}$  and  $2^\circ\text{C}/\text{min}$  (instead of  $10^\circ\text{C}/\text{min}$ ), but little improvement was observed. Although the reason for poor stability is not clear yet, copper cations were responsible for this phenomenon, because Ag-X, which will be discussed next, did not show any degradation of pore structure. It was reported that Nickel exchanged A-zeolite was unstable and lost its crystal structure at a temperature above  $70^\circ\text{C}$ . See Breck, D.W., *Zeolite Molecular Sieves: Structure, Chemistry and Use*; Wiley: New York (1974). The thermal instability of nickel exchanged A-zeolite was interpreted in terms of a ligand-field effect. After dehydration octahedral coordination for the nickel cation is not favored in the zeolite structure. A similar phenomenon might be occurred in copper exchanged X-zeolite.

**Ag-X.** Thiophene adsorption performance on Ag-X was also examined to understand the effect of additional  $\text{Ag}^+$  at SIII sites. Thiophene adsorption amounts on Ag-Y and Ag-X at  $120^\circ\text{C}$  were compared in Figure 8. Contrary to our expectation, Ag-X adsorbed less thiophene than Ag-Y on a per weight basis. However, since Ag-Y and Ag-X have different densities due to their different compositions, the adsorption amounts of thiophene were nearly the same based on per unit cell of faujasite (i.e., about 25 thiophene molecules/u.c. at  $2.3 \times 10^{-5}$  atm and 36 – 40 thiophene molecules/u.c at  $1.8 \times 10^{-2}$  atm for both Ag-Y and Ag-X). The reason for the ineffectiveness of extra  $\text{Ag}^+$  at SIII site in Ag-X is not known. The thiophene adsorption amounts were also examined from the viewpoint of zeolite pore volume and liquid thiophene volume. The molar density of

liquid thiophene is calculated to be 83 cc/mol at 120°C. 1.5 mmol thiophene adsorbed per gram of Ag-Y at  $2.3 \times 10^{-5}$  atm corresponded to 0.125 cc liquid thiophene per gram of Ag-Y. The thiophene liquid volume of 0.125 cc was nearly one half of pore volume of Ag-Y (0.24cc/g as shown in Figure 4), suggesting that one half of the pore was filled with thiophene. Therefore, it does seem likely that the cavity of Ag-X was filled with thiophene even at  $2.3 \times 10^{-5}$  atm and a small amount could be further adsorbed at higher pressures. One possible reason for the relatively low amounts in Ag-X is that thiophene molecules adsorbed could be located at positions near more than one silver cations at both SII and SIII sites simultaneously, so that no improvement in adsorbed amount was observed.

Silver in Ag-X is known to form silver cluster at elevated temperature. Hutson et al. showed that nitrogen adsorption capacity on Ag ion-exchanged low-silica X-zeolite (Si/Al = 1) was enhanced by heating in vacuum at 450°C for more than 4 hours. This enhancement was explained by thermally induced Ag cation and/or cluster migration using Rietvelt refinement of neutron powder diffraction data. The thiophene adsorption isotherm on Ag-X(Si/Al = 1.25) after 450°C for 4 hours is also shown in Figure 5. No enhancement was observed for thiophene adsorption on Ag-X(Si/Al = 1.25).

**H-USY.** Thiophene and benzene isotherms on H-USY(Si/Al = 195) are shown in Figure 9. The interaction between thiophene/benzene and high-silica H-USY was very weak. Neither thiophene nor benzene was adsorbed at pressures lower than  $1 \times 10^{-3}$  atm. Adsorbed amounts were substantially smaller than Na-Y even at  $2 \times 10^{-2}$  atm. These results are clearly due to the strong interactions between the cations in zeolite and the thiophene or benzene molecule.

**Na-ZSM-5.** As stated above, several groups used Na-ZSM-5 for thiophene/benzene purification and showed that Na-ZSM-5 could remove thiophene impurities from benzene in their fixed bed breakthrough experiments. Figure 10 shows isotherms on Na-ZSM-5. Although thiophene and benzene isotherms turned out to be virtually the same on Na-ZSM-5, it may be important to note that thiophene isotherms were fairly flat over the pressure range in the application of purification. This small difference of adsorbed amounts at  $3 \times 10^{-5}$  atm and  $2 \times 10^{-2}$  atm was preferable for the purification of benzene by removal of thiophene, which will be discussed below. One disadvantage of Na-ZSM-5 was small adsorption capacity owing to the small pore volume, as clearly seen in Figure 4.

**Activated carbon and modified activated alumina.** The thiophene and benzene adsorption isotherms on activated carbon (Type PCB) and modified activated alumina (Selexsorb CDX) are shown in Figure 11 and Figure 12. PCB activated carbon is commercially designated for use in liquid phase or vapor phase applications such as

recovery of alcohols, chlorinated hydrocarbons, hydrocarbons and aromatics. Selexsorb CDX is specially formulated by Alcoa Industrial Chemicals for adsorption of polar organic compounds including sulfur-based molecules (mercaptans, sulfides, disulfides, thiophenes), nitrogen-based molecules (nitriles, amines, pyridines) and oxygenated hydrocarbon molecules (alcohol, glycols, aldehydes, ketones, ethers, peroxides). More benzene than thiophene was adsorbed on both activated carbon and modified activated alumina at pressures below  $1 \times 10^{-2}$  atm. This is surprising because Selexsorb was thought to adsorb thiophene more selectively than benzene. This result indicates that polarizability may play a more important role (than permanent dipole moment and magnetic susceptibility) in adsorption on these two sorbents. At pressures higher than  $1 \times 10^{-2}$  atm, pore filling dominated hence benzene adsorbed less than thiophene because of the larger molar volume of benzene than thiophene.

**Comparison of thiophene adsorption on all sorbents.** Thiophene adsorption isotherms on all sorbents are compared in Figure 13. It is clearly seen that Ag-Y and Cu-Y could adsorb significantly larger amounts of thiophene even at very low pressures.

**Heat of adsorption.** Heats of adsorption were calculated using the Clausius-Clapeyron equation from isotherms at two different temperatures, and are shown in Table 7. All the heats of thiophene/benzene adsorption had the tendency to decrease as the loading increased. This is a common phenomenon for the sorbents such as ion-exchanged zeolites that have heterogeneous sites. The heats of adsorption on activated carbon, in particular, ranged widely from 23.9 kcal/mol (at 0.5 mmol/g loading) to 8.0 kcal/mol (at 3 mmol/g). Ag-Y and Cu-Y exhibited the higher heats of adsorption than Na-Y for both benzene and thiophene, it is believed due to  $\pi$ -complexation. More importantly, the heats of adsorption for thiophene were higher than that of benzene. These experimental results can be explained by molecular orbital calculation and NBO analysis, which will be discussed shortly.

At the low loading of 0.5 mmol/g, Na-ZSM-5 showed nearly the same heats of adsorption as Na-Y for both thiophene and benzene. The different pore dimensions (5.2-5.6 Å for ZSM-5 vs. 7.4 Å for Na-Y) apparently had no influence on the heats of adsorption. It is not clear why the amounts adsorbed on Na-Y decreased sharply at very low pressures while that on Na-ZSM-5 maintained.

**Table 7. Heat of adsorption (kcal/mol) calculated from isotherms at different temperatures.**

	Na-Y (Si/Al=2.43)	Ag-Y (Si/Al=2.43)	Cu-Y (Si/Al=2.43)	H-USY (Si/Al=195)	Na-ZSM5 (Si/Al=10)	Activated Carbon Type PCB	Activated Alumina Selexsorb CDX
Thiophene	19.1-19.6 (0.5-2.0)	21.3-21.5 (1.5-1.7)	20.8-22.4 (2.0-3.0)	7.9-11.2 (0.1-0.3)	18.6-19.2 (0.45-0.60)	8.0-23.9 (0.5-3.0)	16.1-17.5 (0.2-1.0)
Benzene	17.0-18.2 (1.5-2.0)	19.0-20.1 (1.5-1.8)	19.3-21.8 (1.8-2.5)	6.6-13.1 (0.1-0.5)	16.5-17.9 (0.45-0.65)	13.1-16.1 (1.0-3.0)	16.8-19.6 (0.6-1.0)

\*) Numbers in parentheses indicate the adsorption amounts (mmol/g) for calculation.

\*\*) The heats of adsorption decreased with loading in all cases.

5

**Bond Energies, Geometries and NBO results.** The energies of adsorption calculated using equations 1 and 2 for thiophene and benzene are summarized in Table 8. The theoretical calculations indicate that the  $\pi$ -complexation strengths follow the order  $\text{CuZ} > \text{AgZ}$  and more importantly, thiophene  $>$  benzene. This trend is in agreement with the experimental data, in Table 7. In fact, the molecular orbital results on CuZ and AgZ are in excellent agreement with the experimental data. Both chloride and zeolite models were used as the anion in the theoretical calculations, while a zeolite framework was the anion in the experiment. It is believed that the anion has a large effect on the  $\pi$ -complexation bonds. The bond energies on the zeolites (Z) are significantly higher than that on the chlorides (Table 8). This result indicates that the zeolite anion is more electronegative than the chloride anion, which has been revealed by Chen and Yang in their ab initio molecular orbital calculations. In the optimized structures of thiophene-MCl complexes, the distance between the thiophene molecule and Cu ion is about 0.3 Å shorter than that of thiophene and Ag ion for chloride. The NBO analysis is summarized in Tables 9 and 10. There is some donation of electron charges from the  $\pi$ -orbital of thiophene to the vacant s orbital of metals known as  $\sigma$  donation and, simultaneously, back-donation of electron charges from the d orbitals of metals to  $\pi^*$  orbital (i.e., anti-bonding  $\pi$  orbital) of thiophene or  $\pi$  back-donation. It appears that the  $\sigma$  donation is more predominant for thiophene and the  $\pi$  back-donation is more important for benzene. Comparing the two anions, zeolite anion and chloride anion, the NBO results show that both  $\sigma$  donation and d -  $\pi^*$  back-donation are significantly stronger with the zeolite anion bonded to  $\text{Ag}^+$  or  $\text{Cu}^+$ . The charge transfer results again confirmed the experimental data that the relative strengths of the  $\pi$ -complexation bonds follow the order: thiophene  $>$  benzene and  $\text{Cu}^+ > \text{Ag}^+$ .

30

**Table 8. Summary of energies of adsorption for thiophene and benzene in kcal/mol calculated from molecular orbital theory (Z denotes Zeolite anion)**

	$E_{\text{ads}}(\text{Thiophene})$	$E_{\text{ads}}(\text{Benzene})$
CuCl	13.5	12.4
AgCl	9.0	8.6
CuZ	21.4	20.5
AgZ	20.0	19.1

**5 Table 9. Summary of NBO analysis\* of  $\pi$ -complexation between thiophene and MCl/MZ**

MX	C-M interaction ( $\sigma$ donation) $q_1$	M-C interaction ( $d - \pi^*$ back-donation) $q_2$	Net Change $q_1 + q_2$
CuCl	0.037	-0.022	0.015
AgCl	0.022	-0.014	0.008
CuZ	0.112	-0.063	0.049
AgZ	0.101	-0.086	0.015

\*  $q_1$  is the amount of electron population change in valence s orbitals of the metal, and  $q_2$  is the total amount of electron population decrease in valence d orbitals of the metal.

**10 Table 10. Summary of NBO analysis\* of  $\pi$ -complexation between benzene and MCl/MZ.**

MX	C-M interaction ( $\sigma$ donation) $q_1$	M-C interaction ( $d - \pi^*$ back-donation) $q_2$	Net Change $q_1 + q_2$
CuCl	0.011	-0.013	-0.002
AgCl	0.003	-0.007	-0.004
CuX	0.078	-0.119	-0.041
AgX	0.043	-0.045	-0.002

\*  $q_1$  is the amount of electron population change in valence s orbitals of the metal, and  $q_2$  is the total amount of electron population decrease in valence d orbitals of the metal.

**15 Uptake Rates.** Table 11 compares diffusion time constants for Ag-Y, Cu-Y and Na-Y. These constants were calculated from the uptake rates using the solution for Fick's law. Uptake rates among the three sorbents were very similar and no notable differences between thiophene and benzene were observed. These rates are reasonably fast for practical applications.

**20** In this experiment, vapor-phase benzene/thiophene adsorption isotherms were investigated to develop new sorbents for desulfurization. Among the sorbents studied, it was found that Cu-Y and Ag-Y exhibited excellent adsorption performance (capacities and separation factors) for desulfurization. This enhanced performance compared to Na-Y is believed to be due to the  $\pi$ -complexation with  $\text{Cu}^+$  and  $\text{Ag}^+$ .

**25** Molecular orbital calculations confirmed the relative strengths of  $\pi$ -complexation: thiophene > benzene and  $\text{Cu}^+ > \text{Ag}^+$ . In an actual desulfurization process, liquid phase

adsorptions such as batch adsorption or fixed-bed adsorption column around RTs are viable options. Liquid phase experiments are described herein. Even in the case of liquid phase separation, enhanced selectivities based on  $\pi$ -complexation studied in this experiment are applicable.

5

**Table 11. Diffusion Time Constants (1/s) of Thiophene and Benzene.**

	Thiophene Pressure Change (atm)	$D/r^2$ (1/s)	Benzene Pressure Change (atm)	$D/r^2$ (1/s)
Ag-Y	1.9E-5 - 1.6E-4	2.0E-05	5.7E-5 - 5.5E-4	5.4E-05
	5.6E-4 - 1.8E-3	3.3E-04	5.5E-4 - 5.4E-3	1.8E-04
	1.8E-3 - 1.5E-2	1.2E-04	5.4E-3 - 2.6E-2	4.2E-04
Cu-Y	2.3E-5 - 8.8E-5	1.3E-05	3.2E-5 - 1.2E-4	2.0E-05
	8.8E-5 - 4.0E-4	2.3E-05	1.2E-4 - 5.4E-4	5.2E-05
	4.0E-4 - 2.2E-3	1.5E-04	5.4E-4 - 3.0E-3	3.3E-04
	2.2E-3 - 1.3E-2	1.4E-04	3.0E-3 - 1.8E-2	3.7E-04
Na-Y	8.8E-5 - 4.0E-4	1.7E-05	0 - 1.5E-4	1.5E-05
	4.0E-4 - 2.2E-3	1.6E-04	1.5E-4 - 5.5E-4	2.6E-05
	2.2E-3 - 1.3E-2	2.8E-04	5.5E-4 - 5.4E-3	5.6E-05
	1.3E-2 - 2.9E-2	5.4E-04	5.4E-3 - 2.6E-2	2.4E-04

## EXPERIMENT D

As mentioned hereinabove, it has further been fortuitously found that the sorbents of the present invention also are excellent sorbents for removal of aromatics. A detailed description of removal of aromatics follows.

Adsorption of benzene and cyclohexane on various Y-zeolites was investigated in order to develop sorbents for the purification of aliphatics by removal of aromatics. It is to be understood that other zeolites, such as zeolite X, zeolite LSX, MCM-41 zeolites, silicoaluminophosphates, and mixtures thereof may also be used in the removal of aromatics. Ag-Y showed superior benzene/cyclohexane selectivities than Na-Y, Pd-Y and H-USY. Separation factors greater than  $10^5$  were obtained with Ag-Y at low concentrations of benzene. The high selectivities were achieved by the strong interaction between benzene and Ag-Y, while the interaction with cyclohexane was not influenced by the cations. Molecular orbital calculation revealed that benzene formed classical  $\pi$ -complexation bond with Ag-Y: donation of electron charges from the  $\pi$ -orbitals of benzene to the vacant s-orbital of the silver ( $\sigma$  donation) and, simultaneously, back-donation of electron charges from d-orbitals of silver to  $\pi^*$  orbital of benzene ( $d-\pi^*$  back-donation). Grand canonical Monte Carlo simulations were also performed for the adsorption isotherms. Potential parameters of benzene on Ag-Y including  $\pi$ -complexation were first developed. GCMC simulation and experiments were in excellent agreement for adsorption of benzene on Y-zeolites.

Purification of aliphatics by removing aromatics is important in both petrochemical industry and for pollution control. Because benzene (and aromatics) is known to be highly carcinogenic, concentration of benzene needs to be minimized in the automotive fuel. A number of separation processes have been employed to reduce the benzene concentration in a refinery's gasoline pool, so that it meets new reformulated gasoline requirements. In a typical benzene reduction process, a combination of extraction and distillation is used. Also, removal of aromatics from kerosene improves the clean burning properties of the fuel and separation of the aromatics from the isoparaffins and naphthenes in lubricating oils improves the viscosity-temperature relationship.

Because of the importance of aromatics/aliphatics separation and the problems associated with current separation processes, possible alternatives have been under continuing investigation. These include pervaporation, liquid membranes, and the use of liquid inclusion complexes. Purification of dilute aromatics from aliphatics (e.g., toluene and/or xylene in heptane) by temperature swing adsorption (TSA) was studied in the liquid phase. Commercially available sorbents were used: silica gel, activated alumina, activated carbon, zeolite 13X, and polymeric resin (XAD-7). Among these sorbents, silica gel was considered the best due to its superior thermal-exchange capacity. However, the selectivities were low.

Adsorption is playing an increasingly important role in separations. However, its utility is limited by the availability of selective sorbents. The conventional sorbents and separations using them are based on van der Waals and electrostatic interactions between the sorbate and the sorbent. Chemical complexation bonds are generally stronger than van der Waals interactions, yet weak enough to be reversible. Therefore, opportunities exist for developing new sorbents and applications in separations by using weak chemical bonds, including various forms of complexation bonds, including  $\pi$ -complexation bonding.

More recently, several new sorbents based on  $\pi$ -complexation were prepared for selective olefin adsorption. These included  $\text{Ag}^+$ -exchanged resins, monolayer  $\text{CuCl}$  on pillared clays and monolayer  $\text{AgNO}_3$ . Moreover,  $\text{Ag}$  ion-exchanged Y-Zeolite was developed to purify butene by removing trace amounts of butadiene. The purification performance of this sorbent was superior to that of NaY owing to  $\pi$ -complexation.

It is possible, in principle, to purify aromatics from aliphatics based on  $\pi$ -complexation. In the benzene molecules, the carbon atom is  $\text{sp}^2$  hybridized. Hence, each carbon has three  $\text{sp}^2$  orbitals and another  $\text{P}_z$  orbital. The six  $\text{P}_z$  orbitals in the benzene ring form the conjugative  $\pi$  bonds. The  $\text{P}_z$  orbitals also form the antibonding  $\pi^*$  orbitals, which are not occupied. When benzene interacts with transition metals, the  $\pi$ -orbitals of benzene could overlap with the empty or unfilled outer-shell s orbital of the transition



metal to form a  $\sigma$ -bond. Furthermore, the vacant antibonding  $\pi^*$ -orbitals of benzene could overlap with the d-orbitals in the transition metals, similar to that formed in the olefin- $\text{Cu}^+$  bond. In this work,  $\text{Ag}^+$  and  $\text{Pd}^{2+}$  ion-exchanged zeolites were selected for the study of aromatics/aliphatics separations, since these two cations have the most promising  
5  $\pi$ -complexation capabilities, and they are stable. In order to understand the effects of  $\pi$ -complexation,  $\text{Ag}^+$  and  $\text{Pd}^{2+}$  ion-exchanged zeolites were compared with that of  $\text{Na}^+$  ion-exchanged zeolite and a high- $\text{SiO}_2$  zeolite.

Benzene and cyclohexane are an ideal pair of model compounds for studying selective sorbents for purification. These molecules have similar shapes,  
10 polarizabilities and volatilities (the boiling points are  $80^\circ\text{C}$  for benzene and  $81^\circ\text{C}$  for cyclohexane). The kinetic diameter of benzene, which is calculated from the minimum equilibrium cross-sectional diameter, is estimated to be 5.85 angstrom compared with 6.0 angstrom for cyclohexane. Therefore, benzene and cyclohexane were used in this work.

In addition to the experimental investigation, molecular orbital calculations  
15 were performed to obtain a basic understanding of the origin of the strong interactions of Ag ion-exchanged zeolite with benzene. Moreover, grand canonical Monte Carlo (GCMC) simulations were used to simulate/predict the isotherms. Many GCMC studies have been performed for predicting adsorption isotherms in zeolites. These include  $\text{N}_2$ ,  $\text{O}_2$ , Ar, Xe,  $\text{CH}_4$ ,  $\text{C}_2\text{H}_4$  and  $\text{C}_4\text{H}_{10}$  on zeolite-A, X, Y and MFI-type Zeolite. Adsorption of  
20 benzene on NaY, Heulandite and MFI-type zeolites has also been studied. However, these studies did not involve the effects of  $\pi$ -complexation on adsorption. In this study, benzene adsorption isotherms on Ag ion-exchanged Y-zeolite were simulated.

### Experimental Details

25 **Sorbent Preparation.** The sorbents in this work were ion-exchanged zeolites. From earlier results on olefin/paraffin separations,  $\text{Ag}^+$  and  $\text{Pd}^{2+}$  were the most promising ions because of their strong  $\pi$ -complexation abilities.

Ion-exchange of zeolites was accomplished with aqueous solutions. Faujasite was selected as the zeolite framework structure for ion-exchange, because of its  
30 large pore aperture (7.4 angstrom), large pore volume (0.489 ml/ml) and wide range of  $\text{SiO}_2/\text{Al}_2\text{O}_3$  ratios (1- $\infty$ ). Two as-received zeolites, Na-type Y-Zeolite (Na-Y, Si/Al=2.43, Strem Chemical) and H-type ultra-stable Y-Zeolite (H-USY, Si/Al=195, TOSOH CORPORATION, HSZ-390HUA), were used in this study.  $\text{Pd}^{2+}$  type Y-Zeolite was prepared by exchanging Na-Y zeolite with  $\text{Pd}(\text{NO}_3)_2$  (Aldrich) in an aqueous solution (Li  
35 et al., 1994). First, Na-Y was exchanged using 2-fold excess of  $\text{Pd}(\text{NO}_3)_2$  (0.005M) at  $80^\circ\text{C}$  for 24 hours. After the exchange, the zeolite suspension was filtered and washed with copious amount of deionized water. The product was dried at  $110^\circ\text{C}$  overnight in air.

$\text{Ag}^+$  ion-exchange was prepared at RT for 24 hours in the same manner as  $\text{Pd}^{2+}$  exchange, using 2-fold excess  $\text{AgNO}_3$  (0.1M).

**Adsorption Isotherms and Uptake Rates.** Single component isotherms for benzene and cyclohexane were measured using standard gravimetric methods. A Shimadzu TGA-50 automatic recording microbalance was employed. Helium (Pre-purified grade, Metro Welding, 99.995%) was used as the carrier gas and was first passed through two consecutive gas-wash bottles (to ensure saturation) which contained benzene (HPLC grade, Sigma-Aldrich, 99.9+%) or cyclohexane (HPLC grade, Aldrich, 99.9+%). After diluting the concentration to the desired value by blending with additional helium (total flowrate: 250 cc/min), the mixture was directed into the microbalance.

Isosteric heats of adsorption were calculated using the Clausius-Clapeyron equation from isotherms at different temperatures. Nitrogen isotherms at 77K measured with a Micromeritics ASAP 2010 system were used for pore size distribution and pore volume determination. Pore size distributions were calculated with Horvath-Kawazoe equation. Pore volumes were calculated at 0.95 P/Po. The overall diffusion time constants,  $D/r^2$ , were calculated from the uptake rates. In this work, the short time region was used.

**Molecular Orbital Calculation Details.** The  $\pi$ -complexation bonding between olefins and sorbents have been extensively investigated using molecular orbital (MO) calculations. More recently, MO studies were extended to benzene adsorption on various salts such as CuCl and AgCl. In this work, similar MO studies for benzene adsorption on Ag ion-exchanged zeolite were performed using a cluster model of Ag-zeolite. The Gaussian 94 Program in Cerius2 molecular modeling software from Molecular Simulation, Inc. was used for calculations. MO calculations for benzene and Ag zeolite were performed at the Hartree-Fock (HF) and density functional theory (DFT) level. The 3-21G basis set is the split-valence basis set, which has been used successfully for many simulations for benzene adsorption on zeolites, protonation reaction of propylene and isobutene on zeolite and  $\text{O}_2$ ,  $\text{N}_2$  and  $\text{C}_2\text{H}_4$  adsorption on Ag-Zeolites. The reliability of this basis set has been confirmed by the accuracy of calculation results in comparison with experimental data. Therefore, the 3-21G basis set was employed for both geometry optimization and natural bond orbital (NBO) analysis.

**Geometry Optimization and Energy of Adsorption Calculations.** The restricted Hartree-Fock (RHF) theory at the 3-21G level basis set was used to determine the

geometries and the bonding energies of benzene on Ag zeolite cluster, since  $\text{Ag}^+$  has filled d-orbitals with spin = 1.

The computational model used for Ag zeolite were the same as that used by Chen and Yang (1996), since this model yielded heats of adsorption of  $\text{N}_2$  and  $\text{C}_2\text{H}_4$  on Ag zeolite that agreed well with experimental data. The simplest cluster model,  $(\text{HO})_3\text{Si}-\text{O}(\text{Ag})-\text{Al}(\text{OH})_3$ , was chosen for this work. The optimized structures were then used for bond energy calculations according to the following expression:

$$E_{\text{ads}} = E_{\text{adsorbate}} + E_{\text{adsorbent}} - E_{\text{adsorbent-adsorbate}} \quad (2)$$

Where  $E_{\text{adsorbate}}$  is the total energy of benzene,  $E_{\text{adsorbent}}$  is the total energy of the bare adsorbent i.e., the Ag zeolite cluster, and  $E_{\text{adsorbent-adsorbate}}$  is the total energy of the adsorbate/adsorbent system.

**Natural Bond Orbital (NBO) Analysis.** The optimized structures were also used for NBO analysis at the B3LYP/3-21G level. The B3LYP (Becke, 1993a) approach is one of the most useful self-consistent hybrid (SCH) approaches (Becke, 1993b), which is Becke's 3-parameter nonlocal exchange functional (Becke, 1992) with the nonlocal correlation functional of Lee, Yang and Parr (1988).

The NBO analysis performs population analysis pertaining to the localized wave-function properties. It gives a better description of the electron distribution in compounds of high ionic character, such as those containing metal atoms (Reed et al., 1985). It is known to be sensitive for calculating localized weak interactions, such as charge transfer, hydrogen bonding and weak chemisorption. Therefore, the NBO program was used for studying the electron density distribution of the adsorption system.

**Monte Carlo Simulation Details.** Grand canonical ensemble (at a fixed pressure) Monte Carlo simulation was performed utilizing the Cerius2 molecular modeling software on a Silicon Graphics Indigo2 workstation running IRIX v.6.5. After the "crystal builder" module was used to set up the zeolite models, energy expressions and parameters for force field were input by the "force field editor" module. The "sorption" module was then used for benzene adsorption simulations.

The simulation was performed at 120°C and 180°C for at least 1,000,000 configurations. During the simulation, the sorbate molecules interacted with the potential field generated by sorbate-sorbent and sorbate-sorbate interactions. The initial configurations contained no sorbate molecules. Each subsequent configuration was generated by one of four moves: CREATE, DESTROY, TRANSLATE and ROTATE.

Molecular creation attempts were made at random points within the accessible portion of the zeolite lattice with the criterion that there be no overlapping sites (i.e., creations which results in interaction sites which were closer than half the sum of the van der Waal's radii of the two sites were rejected). Translation and rotation were performed with the same rejection criterion. For non-overlapping sites, the change in the potential energy accompanying the new configuration was calculated and subsequently accepted or rejected in accordance with standard acceptance probabilities.

**Zeolite Models.** The structure determined from powder neutron diffraction data by Fitch et al. was used as the structure for Na-Y Zeolite (Si/Al=2.43). The location of the Na cations were 32 atoms on SII sites, 16 atoms on SI sites and 8 atoms on SI' sites. Na cations on SI and SI' sites were located in such a manner that two adjacent SI and SI' were not simultaneously occupied. This is due to the electrostatic repulsion caused by their small separation of 0.218 nm. The position of Al in the framework was randomly chosen using the "disorder" function in the "crystal builder" module that obeyed the Loewenstein rule. No charge-free "blocking atom" was added because large molecules such as benzene were not located in the site, which was actually sterically inaccessible.

For the simulation of Ag ion-exchanged zeolite (Si/Al=2.43), the Na cations in Na-Y were replaced by Ag maintaining the same cation locations. An all silica Y-Zeolite structure was used to simulate Ultra-Stable Y-Zeolite (Si/Al=195) since this zeolite has less than one Al atom per unit cell.

Until recently, the location of the Ag cation was not accurately determined. Using neutron diffraction data, Hutson et al (Hutson et al., 2000) reported the Ag location and occupancies of Ag in Ag-Y (Si/Al=2.43) after 450°C dehydration. Their results showed that the Ag cation sites were 28 atoms on SII sites, 4 atoms on SII' site, 11 atoms on SI sites and 12 atoms on SI' sites. Simultaneous occupancy of Ag cations at SII and SII' as well as SI and SI' sites was unlikely due to the large repulsion. This location is very similar to the location of Na cations in Na-Y reported by Fitch et al., 1986. Therefore, the zeolite model for Ag-Y used in this work is considered to reflect the actual Ag cation locations in Ag-Y (Si/Al=2.43).

**Forcefield Determination.** One of the most important factors for GCMC simulation is the selection of an energy expression and parameters for the forcefield. The forcefield used in these simulations was a modified version of Cerius2 Sorption Demontis Forcefield, since Demontis et al. simulated the mobility of benzene in Na-Y zeolite successfully using molecular dynamics methods. In this model, the total potential energy ( $U_{Total}$ ) between the zeolite lattice and adsorbate molecules is written as the sum of the interactions between

adsorbate molecules(AA) and that between the adsorbate molecules and the zeolite lattice (AZ).

$$U_{Total} = U_{AA} + U_{AZ} \quad (3)$$

5

Interactions between adsorbate molecules ( $U_{AA}$ ) were described as the sum of the atom-atom Buckingham potentials (the first and second terms below), which have shown to yield reasonable predictions for liquid and solid benzene, and the Coulombic interaction potentials (the third term below).

10

$$U_{ij} = A_{ij} \exp(-B_{ij}r_{ij}) - \frac{C_{ij}}{r_{ij}^6} + \left( \frac{q_i q_j}{r_{ij}} \right) \quad (4)$$

The first and second terms represent, respectively, the repulsive and dispersive potential energies between sites “i” and “j”, and the third term represents the interaction potential between point charges  $q_i$  and  $q_j$  of sites “i” and “j” separated by a distance  $r_{ij}$ .

15

The interactions between the adsorbate molecules and the zeolite lattice ( $U_{AZ}$ ) is written as the sum of the atom-atom Lennard-Jones 12-6 potential and the Coulombic interaction potentials.

20

$$U_{ij} = 4\varepsilon_{ij} \left[ \left( \frac{\sigma_{ij}}{r_{ij}} \right)^{12} - \left( \frac{\sigma_{ij}}{r_{ij}} \right)^6 \right] + \left( \frac{q_i q_j}{r_{ij}} \right) \quad (5)$$

Following the empirical approach used by Razman and Hall (1991), Watanabe et al. (1995) used the empirical approach to parameterize the forcefield for adsorption of  $N_2$ ,  $O_2$ , and Ar in type A and faujasite zeolites. The dispersive part of the Lennard-Jones 12-6 potential ( $U_{dispersion}$ ) was written using an adjustable parameter ( $\beta_i$ ) of the adsorbate and the polarizabilities ( $\alpha$ ) of the atoms of the adsorbate molecules (i) and in the zeolite lattice (j).

25

$$U_{dispersion} = -\beta_i \left( \frac{\alpha_i \alpha_j}{r_{ij}^6} \right) \quad (6)$$

The potential energy well depth parameter,  $\varepsilon_{ij}$ , is then written as

30

$$\varepsilon_{ij} = \beta_i \left( \frac{\alpha_i \alpha_j}{4\sigma_{ij}^6} \right) \quad (7)$$

The Lennard-Jones parameter,  $\sigma_{ij}$ , for the adsorbate-zeolite interaction is given by the mixing rule,

$$\sigma_{ij} = \left( \frac{\sigma_i + \sigma_j}{2} \right) \quad (8)$$

The  $\sigma_j$  for the zeolite lattice are related to the van der Waals radii,  $R_j$ , of the respective ions by

$$R_j = 2^{1/6} \sigma_j \quad (9)$$

The well depth parameter,  $\epsilon_{ij}$ , is assumed to be a geometric combination of  $\epsilon_i$  and  $\epsilon_j$ ,

$$\epsilon_{ij} = (\epsilon_i \epsilon_j)^{0.5} \quad (10)$$

The van der Waals energy in the periodic framework was calculated using a minimum image convention with an interaction cut-off distance of 1 nm. The Coulombic term was evaluated using the Ewald summation method.

The potential parameters used for Na-Y, Ag-Y and H-USY are listed in Table 12. The potential parameters for Na-Y are the same as that of Demontis et al. (1989). Van der Waals interactions between adsorbate and zeolite cage were modeled by means of interactions between the (C,H) and (Na,O) atoms. Interactions with the Si and Al atoms were neglected because they were well shielded by the oxygen atoms of the  $\text{SiO}_4$  and  $\text{AlO}_4$  tetrahedra. Electrostatic interactions between all charges were included in the potential energy calculation. As for Ag-Y and all silica Y zeolites, modification of parameters was performed using the mixing rule and the geometric combination rule. The detailed scheme for parameterization will be discussed shortly.

**Table 12. The Potential Parameters used for Na-Y, Ag-Y and H-USY**

Na-Y	$U_{AA}$ <sup>1)</sup>	C-C	H-H	C-H	
	A(kcal/mol)	88371	2861	15901	
	B(1/Å)	3.60	3.74	3.67	
	C(A <sup>6</sup> *kcal/mol)	583.13	32.60	137.88	
	$U_{AZ}$	O-C	O-H	Na-C	Na-H
	$\epsilon$ (kcal/mol)	0.25547	0.16515	0.04187	0.03153
	$\sigma$ (Å)	2.9984	2.5893	3.3279	2.7651
Ag-Y (Case 1)	$U_{AZ}$	O-C	O-H	Ag-C	Ag-H
	$\epsilon$ (kcal/mol)	0.25547	0.16515	<u>0.7823</u>	<u>0.5895</u>
	$\sigma$ (Å)	2.9984	2.5893	<u>3.5773</u>	<u>3.0145</u>
Ag-Y (Case II)	$U_{AZ}$	O-C	O-H	Ag-C	Ag-H
	$\epsilon$ (kcal/mol)	0.25547	0.16515	<u>0.7601</u>	<u>0.5728</u>
	$\sigma$ (Å)	2.9984	2.5893	<u>3.5773</u>	<u>3.0145</u>
H-USY	$U_{AZ}$	O-C	O-H		
	$\epsilon$ (kcal/mol)	<u>0.1687</u>	<u>0.1271</u>		
	$\sigma$ (Å)	2.9984	2.5893		

1) Parameters for  $U_{AA}$  are the same for all sorbents.

2) The numbers with underline were determined in this work.

5

**Assignment of charges for adsorbate and adsorbent.** Assignment of charges also has a significant impact on simulation results when the Coulombic interactions are not negligible. In this work, the existing model for benzene in Cerius<sup>2</sup> was used. In this model, each carbon in benzene carries -0.093 point charge, while hydrogen carries +0.093. These values were nearly the average values from the various charge determination methods: MOPAC (0.1022), ZINDO (0.072) and charge equilibration method ( $Q_{eq}$ ) by Rappe and Goddard (0.1147).

10

The point charges of zeolite were assigned either by (i) using the point charges in the literature or (ii) calculating by means of the charge equilibration method in the Cerius2 software. In this work, Na, Si/Al, O in Na-Y carried the charges of +0.78, +1.2125 and -0.72, respectively, since these values were successfully used in quantum mechanics simulations. Here, no distinction was made between Si and Al atoms in terms of point charges. Charges of Ag-Y and all-silica Y-Zeolites were calculated by the charge equilibration method: Ag(+0.45), Si/Al(+1.16875), O(-0.65), which will be referred to as **Case I** for Ag-Y, and Si(+1.2650), O(-0.6325) for H-USY. In order to investigate the effect of the assigned charges to the isotherm simulation results, the same charges that were used for Na-Y, i.e., Ag(+0.78), Si/Al(+1.2125) and O(-0.72), were also used for Ag-Y. This case is referred to as **Case II** for Ag-Y. For all cases, regardless of the positions of cations and framework atoms (Si, Al, O), the same values of point charge were assigned to the same atoms throughout the simulation unit cell, even though the point charge might vary with the position of the atom. The Ag cation charges used for Monte Carlo

15

20

25

simulation were also consistent with the values calculated by molecular orbital method at MP2/3-21G (Ag charge : +0.49) or MP2/LanL2DZ level (Ag charge : +0.74) using a zeolite cluster model.

## 5 Results and Discussion - Experimental

**Benzene/cyclohexane adsorption isotherms.** Pure component isotherms of benzene and cyclohexane were measured for H-USY(Si/Al=195), Na-Y(Si/Al=2.43), Ag-Y(Si/Al=2.43), and Pd-Y(Si/Al=2.43) at 120°C and 180°C, shown in Figures 22-25.

Isosteric heats of adsorption calculated using the Clausius-Clapeyron equation are listed in Table 13.

**Table 13. Comparison of Heat of Adsorption (kcal/mol) between Experimental and Simulated Results**

		Na-Y	Ag-Y	H-USY
Benzene	Experimental	17.7-18.2	20.5-20.7	6.2-7.2
	Monte Carlo Simulation	16.4-18.5	18.8-21.1	8.2-9.2
	Molecular Orbital Calculation	***	17.2	***
	Barthomeuf et al. <sup>1)</sup>	17.5-18.0	***	***
Cyclohexane	Experimental	10.9-13.0	12.1-12.3	4.1-4.3
	Barthomeuf et al. <sup>1)</sup>	12.0-13.2	***	***

1) Barthomeuf and Ha, 1973

In the case of H-USY, the adsorbed amounts of cyclohexane were higher than that of benzene at > 0.04 atmosphere. This result qualitatively agreed with calculations using the Horvath-Kawazoe theory. The threshold pore-filling vapor pressures of cyclohexane and benzene at 120°C and 180°C were calculated using the spherical pore model of the H-K method. The threshold pressure is the pressure where the steep rise in the isotherm occurs. At both temperatures, it was found that the pore-filling pressure of cyclohexane was 20% lower than that of benzene. The reason for this difference was the larger polarizability ( $11.0 \times 10^{-24} \text{ cm}^3$  for cyclohexane and  $10.3 \times 10^{-24} \text{ cm}^3$  for benzene) and magnetic susceptibility ( $11.3 \times 10^{-29} \text{ cm}^3$  for cyclohexane and  $9.1 \times 10^{-29} \text{ cm}^3$  for benzene) of cyclohexane. However, the calculated isosteric heat of adsorption of benzene was slightly higher than that of cyclohexane. A possible reason for the larger heat of benzene adsorption was the existence of  $\text{H}^+$  in the zeolite, although the number of proton was extremely small (less than one per unit cell). The interaction between protons in zeolite and  $\pi$ -electrons of benzene might be stronger than the interaction between oxygen in zeolite and benzene. Therefore, the amounts of benzene adsorption were slightly larger than that of cyclohexane at less than 0.04 atm, leading to its higher heat of adsorption.



On all other sorbents investigated in this work, larger amounts of benzene were adsorbed at all pressure ranges. Heats of adsorption for benzene were 18 kcal/mol for Na-Y and 21 kcal/mol for Ag-Y, while heats of adsorption for cyclohexane were 10-12 kcal/mol for both Na-Y and Ag-Y. These results are clearly due to the strong interactions between the cations in zeolite and the benzene molecule. Consequently, Ag-Y and Na-Y could adsorb large amounts of benzene even at the pressure of less than 0.01 atm. The heats of adsorption on Na-Y were comparable to previous work (Barthomeuf and Ha, 1973). Most importantly, Ag-Y showed the strongest interactions for benzene and the largest heats of adsorption (20.5 kcal/mol). For cyclohexane adsorption, the adsorption amounts and heat of adsorption were almost the same between Ag-Y and Na-Y, since  $\pi$ -complexation was absent for cyclohexane. A detailed discussion will be made in the section of molecular orbital calculation and Monte Carlo simulation results. These results indicated that improved purification performance of benzene from cyclohexane is possible using Ag-Y. The isotherms of both Ag-Y and Na-Y are reversible, although it took a little longer time to desorb benzene and cyclohexane. For example, 200 minutes are necessary to desorb benzene completely after the adsorption at 0.1 atmosphere. This slow desorption is clearly due to the strong interaction between benzene and Ag. However, the bonds are of the order of 20 kcal/mol, which are weak enough so a substantial fraction of the adsorbed benzene is desorbed in a few minutes. For practical applications, thermal desorption may be a desirable option.

Pd-Y gave lower adsorption amounts than both Ag-Y and Na-Y. This decrease of adsorption amounts by ion-exchange with Pd was due to degradation of the zeolite structure. In Figure 26, the pore size distributions for all sorbents calculated from  $N_2$  isotherms at 77 K are shown. Pd-Y had a small pore volume with a wide pore size distribution, clearly indicating the collapse of the zeolite pore structure or pore blockage by Pd. The Pd ion-exchanged was performed at 80°C, compared with the Ag ion-exchange at RT. Collapsing of zeolite structure tends to occur considerably more in acidic solution and at higher temperatures. The pore volume of Ag-Y also decreased by 23% after ion-exchange. However, this reduction of Ag-Y was mainly caused by 37% density increase of the zeolite lattice by replacing  $Na^+$  with  $Ag^+$  (27% reduction of pore volume per weight basis). The pore structure of Ag-Y was intact after ion-exchange.

Another interesting phenomenon in Figure 26 is the apparent shift of the pore size distribution in H-USY toward a higher value, compared to other zeolites. This was likely due to the lower polarizability of oxygen in the framework of high- $SiO_2$  zeolites (Pellenq and Nicholson, 1993), which will be discussed in detail in the section of Monte Carlo simulation results. Otherwise, the interactions between nitrogen and cations in zeolites would have led to a shift of the pore sizes toward smaller values for Na-Y, Ag-Y

and Pd-Y. Since the pore sizes of Na-Y, Ag-Y and Pd-Y were the same as the actual value for Y zeolites (1.3nm), the latter explanation is not plausible.

**Diffusion time constants.** In Table 14, diffusion time constants calculated from 0 - 0.3 fractional uptake were summarized. Diffusion time constants of benzene and cyclohexane in Na-Y and Ag-Y were of the order of  $10^{-4}$  1/s. These values were almost the same as those of benzene and cyclohexane into AgNO<sub>3</sub> monolayer dispersed SiO<sub>2</sub> sorbent (Takahashi et al.). However, these values were an order of magnitude lower than those of propylene and propane in AgNO<sub>3</sub> monolayer-dispersed SiO<sub>2</sub> sorbent (Rege, 1998) and at least the same as those of ethylene and ethane into Ag ion-exchanged resins (Wu et al., 1997). The diffusion rates of benzene in these zeolites are high for applications (Yang, 1987).

**Table 14. Diffusion Time Constants of Benzene and Cyclohexane**

Adsorbents	Temp. (°C)	Benzene (1/s)	(Pressure Change) (atm)	Cyclohexane (1/s)	(Pressure Change) (atm)
Na-Y	120	$2.1 \times 10^{-4}$	$(5.4 \times 10^{-3} \rightarrow 2.6 \times 10^{-2})$	$9.8 \times 10^{-4}$	$(1.1 \times 10^{-2} \rightarrow 2.0 \times 10^{-2})$
Ag-Y	120	$4.2 \times 10^{-4}$	$(5.4 \times 10^{-3} \rightarrow 2.6 \times 10^{-2})$	$1.1 \times 10^{-4}$	$(2.0 \times 10^{-3} \rightarrow 3.7 \times 10^{-2})$
AgNO <sub>3</sub> /SiO <sub>2</sub> (0.33g/g) <sup>1)</sup>	120	$1.3 \times 10^{-4}$	$(2.0 \times 10^{-3} \rightarrow 3.7 \times 10^{-2})$	$2.9 \times 10^{-4}$	$(1.1 \times 10^{-2} \rightarrow 2.0 \times 10^{-2})$
Adsorbents	Temp. (°C)	Propylene (1/s)	(Pressure Change) (atm)	Propane (1/s)	(Pressure Change) (atm)
AgNO <sub>3</sub> /SiO <sub>2</sub> (0.33g/g) <sup>2)</sup>	70	$3.5 \times 10^{-3}$	$(0 \rightarrow 1)$	***	***
Ag-Amberlyst-35 <sup>3)</sup>	70	$1.5 \times 10^{-4}$	***	$1.4 \times 10^{-4}$	***

1) Takahashi et al., 2000

2) Rege et al., 1998

3) Wu et al., 1997

## Molecular Orbital Calculation

**Adsorption Bond Energy and Molecular Geometries.** Adsorption energy and structural geometry were calculated using molecular orbital theory. The calculated heat of adsorption using B3LYP/3-21G level by equation (1) is also compared with experimental and Monte Carlo simulation results in Table 13. The theoretical value, 17.2 kcal/mol, was in fairly good agreement with the experimental value. The comparison of bond length by benzene adsorption revealed that the Ag-O length increased from 3.023Å to 3.246Å. The C-C bond length in benzene also increased from 1.385Å to 1.385-1.391Å. This trend was consistent with that for benzene interaction with AgCl.

**Natural Bond Orbital (NBO) Results.** The nature of benzene-Ag zeolite interaction can be better understood by analyzing the NBO results. The main feature of the interaction can be seen from the population changes in the vacant outer-shell s orbital of the silver and those in the d orbitals of silver upon adsorption. In Table 15, NBO analysis results for benzene on Ag zeolite are compared with other combinations of adsorbates and adsorbents. According to the electron population changes by benzene adsorption on Ag zeolite, the trend is in agreement with previously reported trend of  $\pi$ -complexation, i.e., donation of electron charges from the  $\pi$ -orbitals of benzene to the vacant s-orbital of the silver ( $\sigma$  donation) and, simultaneously, back-donation of electron charges from the d-orbitals of silver to  $\pi^*$  orbital of benzene (d- $\pi^*$  back-donation). The contribution of d- $\pi^*$  back-donation is larger than  $\sigma$  donation, resulting in the decrease of net electron charge in silver. The net electron charge of carbon in benzene increased instead.

The differences of electron population changes between benzene and ethylene adsorption deserve a discussion. From Table 15, it is seen that the contribution of donation is predominant in ethylene adsorption, while d- $\pi^*$  back-donation is slightly larger in benzene adsorption. Also, the extent of  $\sigma$  donation and d- $\pi^*$  back-donation by benzene adsorption was considerably smaller compared with ethylene adsorption. Therefore,  $\pi$ -complexation with benzene was weaker than that with ethylene. Weak  $\pi$ -complexation of benzene can also be understood by the difference in bond lengths. The bond length between carbon in ethylene and silver in AgCl was 2.66 Å, while that between carbon in benzene and silver in Ag zeolite or AgCl was 2.71-3.7 Å or 3.22 Å, respectively. This longer bond length was caused by the less overlap of orbitals from the weaker  $\pi$ -complexation.

**Table 15. Summary of the NBO Analysis of the  $\pi$ -complexation: Electron Population Changes of Each Orbital After Adsorption**

Method/Basis Set		Silver			Carbon		
		5s	$\Sigma 4d$	Net Change	2s	$\Sigma 2p$	Net Change
Benzene on Ag Zeolite	B3LYP/3-21G	0.00541	-0.0135	-0.00805	0.00554	0.00709	0.01263
Benzene on AgCl <sup>1)</sup>	B3LYP/LanL2DZ	0.0033	-0.0071	-0.0038	***	***	***
C <sub>2</sub> H <sub>4</sub> on Ag Zeolite <sup>2)</sup>	MP2/3-21G	0.0596	-0.0177	0.0419	0.0203	0.0193	0.0396
C <sub>2</sub> H <sub>4</sub> on AgCl <sup>2)</sup>	MP2/3-21G	0.1204	-0.0470	0.0734	0.0226	0.0142	0.0368
C <sub>2</sub> H <sub>4</sub> on AgCl <sup>3)</sup>	B3LYP/LanL2DZ	0.061	-0.055	0.006	***	***	***

1) Takahashi et al., 2000

2) Chen and Yang, 1996

3) Huang et al., 1999

**Monte Carlo Simulation.** Monte Carlo simulation of adsorption isotherms provides great insight into the adsorption mechanism via model construction, charge assignment and

forcefield determination. In this section, benzene adsorption on Na-Y, H-USY and Ag-Y is simulated and the mechanism of adsorption on each zeolite is discussed.

**Na-Y Zeolite.** GCMC simulation results of benzene isotherms at 120 and 180°C using the potential parameters given in Table 12 are shown in Figure 27, where they are also compared with experimental data. The simulation results were in excellent agreement with experimental data. The calculated heats of adsorption were 16.4 - 18.5 kcal/mol, which were in agreement with that from experiments. It was hence confirmed that the energy expressions and parameters were suitable for simulation of benzene isotherms on Na-Y.

**H-USY zeolite.** First, simulation of benzene isotherms on H-USY was attempted using the same potential parameters as on Na-Y. However, the simulated isotherms were considerably higher than the experimental data. This disagreement was caused by incorrect well depth parameters,  $\epsilon_{O-C}$  and  $\epsilon_{O-H}$ , for van der Waals interaction. Pellenq and Nicholson (Pellenq and Nicholson, 1993) reported the values of the polarizabilities of framework atoms in silicalite and aluminosilicates determined from Auger electron spectroscopy data. It was found that the polarizability for oxygen in zeolite framework is sensitive to the ratio of silicon to aluminum and also the nature of the extraframework cations. Watanabe et al. (1995) used different potential values for oxygen in silicalite (0.202 kcal/mol), denoted by  $Oz(Si-O-Si)$ , and that in aluminosilicates (0.334 kcal/mol), denoted by  $Oz(Si-O-Al)$ .

In this work, an adjustment of  $\epsilon_{Oz(Si-O-Si)-C}$  and  $\epsilon_{Oz(Si-O-Si)-H}$  was made to simulate the experimental Henry's law constants at 120°C and 180°C. Here, low pressure data may depend on the benzene-zeolite interactions so the benzene-benzene interactions were neglected. Using the well depth parameter for  $\epsilon_{Na-C} = 0.04187$  kcal/mol and  $\epsilon_{Na-H} = 0.03153$  kcal/mol for Na-Y (in Table 15) and assuming  $\epsilon_{Na} = 0.041$  kcal/mol as used by Watanabe et al. (Watanabe et al., 1995) for Na-A and Na-X,  $\epsilon_C = 0.0428$  kcal/mol and  $\epsilon_H = 0.0243$  kcal/mol were obtained from the geometric combination rule, equation (10). Therefore,  $\epsilon_{Oz(Si-O-Si)-C}$  and  $\epsilon_{Oz(Si-O-Si)-H}$  for H-USY could be expressed as  $(0.0428 \times \epsilon_{Oz(Si-O-Si)})^{0.5}$  and as  $(0.0243 \times \epsilon_{Oz(Si-O-Si)})^{0.5}$ , respectively. By fitting with  $\epsilon_{Oz(Si-O-Si)}$ ,  $Oz(Si-O-Si) = 0.665$  kcal/mol was obtained to fit the experimental Henry's law constant of 0.519 molecules/(cell.kPa) at 120°C and 0.137 molecules/(cell.kPa) at 180°C. The ratio of  $\epsilon_{Oz(Si-O-Si)}$  over  $\epsilon_{Oz(Si-O-Al)}$  was 0.44 (calculated from  $\epsilon_{Oz(Si-O-Al)-H}$ ) - 0.60 (calculated from  $\epsilon_{Oz(Si-O-Al)-C}$ ), which was in agreement with the ratio of 0.60 obtained by Watanabe et al. (Watanabe et al., 1995).

Using the modified parameters for H-USY (in Table 15), the benzene isotherms were calculated and compared with experimental isotherms in Figure 28. Again,

the isotherms and the heat of adsorption (8.2 - 9.2 kcal/mol) obtained from simulation were in excellent agreement with the experimental data.

**Ag-Y zeolite.** The potential parameters for Ag-Y are listed in Table 15. These parameters were modified to get the low pressure points of the isotherm at 180°C (1.30 mmol/g at  $1.6 \times 10^{-4}$  atmosphere), although adjustment of the parameters to fit the experimental Henry's law constant was preferable. The reason not to use the experimental Henry's constant was that the small pressure values ( $8.7 \times 10^{-6}$  atmosphere) at the lowest adsorbed amount in the isotherms might lead to the large error of potential parameters. The procedure of adjustment was basically the same as in the case for H-USY except for changing the  $\epsilon_{Ag}$  value instead of the  $\epsilon_{Oz(Si-O-Si)}$  value.  $\epsilon_C = 0.0428$  kcal/mol and  $\epsilon_H = 0.0243$  kcal/mol were obtained from the geometric combination rule, equation (10). Then,  $\epsilon_{Ag-C}$  and  $\epsilon_{Ag-H}$  for Ag-Y could be estimated from  $(0.0428 \times \epsilon_{Ag})^{0.5}$  and  $(0.0243 \times \epsilon_{Ag})^{0.5}$ , respectively. In **Case I** for Ag-Y,  $\epsilon_{Ag}$  became 14.3 kcal/mol, while  $\epsilon_{Ag} = 13.5$  kcal/mol was obtained for **Case II**. The larger well-depth parameter was needed for Case I to compensate for the weaker Coulombic interaction due to the smaller Ag cation charge. In both cases, the  $\epsilon_{Ag}$  values used were more than 2 orders of magnitude greater than  $\epsilon_{Na}$ , clearly indicating the strong interaction from  $\pi$ -complexation.

Figure 29 shows the simulation results of benzene on Ag-Y for Case I and Case II. The differences between Case I and Case II were fairly small. In both cases, the agreement with experimental isotherms was not as good as that for Na-Y and H-USY. However, they certainly followed the basic trend of the experimental isotherms. The calculated heat of adsorption was 18.8 - 21.1 kcal/mol, which was higher than Na-Y and also in agreement with the experimental value.

In all cases, including Ag-Y, Na-Y, and H-USY, the simulated isotherms tended to be higher than the experimental isotherms in the lower pressure range with few exceptions, while they were lower in the higher pressure range. The higher simulation results at low pressures might be caused by the larger values for the well-depth parameter between oxygen (zeolite) - carbon (benzene) interaction and oxygen (zeolite) - hydrogen (benzene) interaction. The other possible cause was the imperfection of the zeolite crystals. Since zeolites contain defects while in Monte Carlo simulation perfect zeolite lattice was assumed. In the high pressure range, larger experimental values were possibly caused by adsorption between zeolite crystals.

Adsorption sites for benzene on Na-Y and Ag-Y were investigated using the Mass Cloud Plots function in Cerius2 (not shown here). It was confirmed that benzene was adsorbed preferentially near the SII cation sites and the center of the 12-ring window, which was consistent with the neutron diffraction data for Na-Y obtained by Fitch (Fitch et al., 1986). For Ag-Y, benzene was adsorbed slightly further away from the SII cation sites

than that in Na-Y, due to the fact that the van der Waals radius of  $\text{Ag}^+$  is 30% larger than that of  $\text{Na}^+$ .

Figs. 30-32 are graphs depicting further breakthrough curves.

## EXPERIMENT E

**Adsorbent Preparation.** The adsorbents used in this study were copper cation forms of Y Zeolite and also type PCB Activated Carbon (PCB-AC). The former were prepared initially using conventional liquid phase ion exchange techniques. The starting material, sodium type (Na) Y Zeolite (Strem Chemicals, Si/Al = 2.43), was used as received and in powder form. The activated carbon samples were obtained from Calgon Corporation also in powder form and used without further purification.

Cu(I)-Y (or reduced Cu(II)-Y) was prepared by first ion exchanging Na-Y with a  $\text{Cu}(\text{NO}_3)_2$  aqueous solution (0.5 M) for 48 hours followed by reduction of  $\text{Cu}^{2+}$  to  $\text{Cu}^+$ . The amount of copper in the ion exchange solution was equivalent to a 5-fold cation exchange capacity. The adsorbent was recovered by filtration and washed with copious amounts of deionized water, followed by drying at  $100^\circ\text{C}$  for at least 24 hours. Activation was performed at  $450^\circ\text{C}$  in pure helium to promote auto-reduction of  $\text{Cu}^{2+}$  species to  $\text{Cu}^+$ , which is desired for  $\pi$ -complexation (Cu(I)-Y).

**Reagents and Standards.** Gasoline and diesel samples were obtained from British-Petroleum (BP) gas stations located in the Michigan area. Gasoline was unleaded regular type, while diesel is type #2 according to BP's specifications. The average total sulfur concentration for these fuels was reported to be 335 and 430 ppmw, respectively (data available from BP). Thiophene, benzothiophenes (BT), and dibenzothiophene (DBT) standards were purchased from Sigma-Aldrich.

**Fixed-Bed Adsorption/Breakthrough Experiments.** All adsorption/breakthrough experiments were performed in vertical custom made quartz adsorbers equipped with a supporting glass frit. The setup consisted of a low-flow liquid pump equipped with a ceramic piston and cylinder liner, Kynar compression fittings, two Pyrex feed tanks, and a heating element. Initially, the adsorbents were loaded inside the adsorber (between 1 or 2 grams), and heated in situ ( $450^\circ\text{C}$ ) while flowing helium. Temperatures were maintained at steady values using a PID temperature controller. The gases used for activation were pretreated inline prior to contacting the sorbent using a 3A-type zeolite. The latter allows removal of trace water from the gases, which may adsorb in the adsorbents that are being tested. After activation treatment, the adsorbent under study was allowed to cool down to RT under helium and then tapped to ensure proper packing. Next, a sulfur-free

hydrocarbon was allowed to flow downwards through the sorbent at a rate of 0.5 cm<sup>3</sup>/min. After wetting the adsorbent for about 10 minutes, the feed was changed to either commercial grade gasoline or diesel at a 0.5 cm<sup>3</sup>/min rate. Samples were collected at regular intervals until saturation was achieved, which depended on the adsorption  
5 dynamics and amount of adsorbent.

**Gas Chromatography Analysis.** All the samples collected during the breakthrough experiments were analyzed using a Shimadzu GC-17A v3 unit equipped with an EC-5 capillary column (L = 30 m; ID = 0.32 mm) and a flame photometric detector (FPD). The  
10 column temperature program was set to increase from 50°C to a set value at a 5°C/min rate. For gasoline and diesel sulfur analysis, the column final temperature values were 250°C and 330°C, respectively. In addition, a split mode injection was used for all samples at a 100:1 ratio. About 4mL of sample volume was injected for each GC-FPD run. The injection port temperature was set to either 250°C or 330°C, this depending on the nature  
15 of the samples under analysis.

Peak identification information for sulfur compounds present in gasoline and diesel was gathered after using standards and by retention time comparison with data available in the literature. For standards, thiophene, BT and DBT solutions were diluted in sulfur free *n*-octane to a known concentration and then injected for retention time  
20 determination. The total sulfur concentration during breakthrough adsorption experiments for either gasoline or diesel was estimated after integrating the entire GC chromatogram region. It was assumed the total concentration is proportional to the collective areas under the peaks and that it follows a linear fashion. This is believed to be acceptable for conditions where complete sample elution after injection is achieved and after correction  
25 for noise data. The total elution times for gasoline and diesel for the GC conditions described above were 30 and 50 minutes, respectively. A similar procedure was used to calculate individual sulfur components concentration during adsorption experiments. For this purpose, the specific compound unique peak area was used. Figures 33 and 34 show GC-FPD chromatograms for as-received gasoline and diesel fuels. The results are similar  
30 to those found in literature for similar analysis conditions and set-up.

**FTIR Spectroscopy Analysis.** Fuels were analyzed for aromatic/aliphatic C-H bond stretching using FTIR spectroscopy on a Nicolet Impact 400 FTIR spectrometer equipped with a TGS detector. The samples were loaded into a liquid IR cell fitted with ZnSe  
35 windows prior each analysis following standard procedures. The spectra were then taken at RT using 100 scans per run and a resolution of 4 cm<sup>-1</sup>. Background spectra were collected using the liquid IR cell without any sample inside.

## Results and Discussion

**Adsorbent Characterization.** Characterization for the adsorbents used in this study was achieved by NAA. All the zeolites were in hydrated conditions before testing. As seen in Table 16, ion-exchanging Na-Y with  $\text{Cu}^{2+}$  results in an incomplete ion exchange. If it is assumed that one  $\text{Cu}^{2+}$  cation compensates for two aluminum tetrahedra, then in the present case, the ion exchange resulted in 70% substitution of the original sodium ions (i.e.,  $2\text{Cu}/\text{Al} = 0.72$ ). The remaining sodium species were then compensating for the other aluminum tetrahedra; in other words, the  $(2\text{Cu} + \text{Na})/\text{Al}$  ratio should be unity, which is observed here. This scheme may be the simplest one used to describe such behavior.

**Adsorbent Activation, Copper Auto-reduction and Migration.** Since Y zeolite is known to be highly hydrophilic (uptake > 20 wt% water at ambient conditions), all the gases used for activation of the adsorbents were pretreated with 3A-Type zeolites prior to entering the fixed-bed unit. For Cu(II)-Y, the activation was performed at  $450^\circ\text{C}$  in helium to promote auto-reduction of  $\text{Cu}^{2+}$  species to  $\text{Cu}^+$ , which is desired for  $\pi$ -complexation (Cu(I)-Y). After 18 hours of auto-reduction, the color of Cu(I)-Y was pale green, compared to a bluish green typically observed in Cu(II)-Y. This was sure evidence of auto-reduction, as  $\text{Cu}^+$  should result in a white color (like in CuCl). In the present invention, successful liquid phase thiophene adsorption experiments as described hereinabove with Cu(I)-Y zeolites provide further evidence of reduction of  $\text{Cu}^{2+}$ .

The adsorption capacity of auto-reduced Cu-Y observed for simple liquid hydrocarbon mixtures is believed to be due not to the reduction of the copper ions, but also because of the final position of the cations after activation and/or during adsorption.  $\text{Cu}^+$  cations occupy exposed sites in the Y zeolite framework, such as sites II and III according to the nomenclature of Smith in order to interact with the sulfur molecules. Recent studies by Fowkes et al. have shown that, upon reduction of Cu(II)-Y, there was a redistribution of cation positions and most of the reduced species ( $\text{Cu}^+$ ) occupied sites  $\text{I}^*$  and II. Lamberti et al. showed similar results for both reduced Cu(II)-Y and Cu(I)-Y prepared by ion exchange and gas phase reaction with CuCl, respectively. In addition, some  $\text{Cu}^+$  ions could be induced to migrate to more exposed sites under the presence of guest molecules. Turnes-Palomino et al. found, based on IR data, that this happens when CO molecules are adsorbed in Cu(I)-Y. Their zeolite was also prepared by vapor-phase exchange of H-Y with CuCl. Thus, based on Turnes-Palomino's findings, there could also be some synergy that contributes for the observed adsorption capacity of this adsorbent.

**Fixed-Bed Adsorption Tests.** After activating the adsorbents *in-situ*, a solution of either commercial regular gasoline or diesel was passed through the fixed-bed and the



downstream sulfur concentration monitored as a function of time. Figure 35 shows a breakthrough/adsorption profile obtained during desulfurization of gasoline with a Cu(I)-Y adsorbent. Adsorption capacities at both breakthrough and saturation were obtained after integrating for the area above the breakthrough curves. For gasoline treatment with Cu(I)-Y the loadings at breakthrough and saturation were 0.14 and 0.39 mmol/g, respectively (Table 17). In the present invention, breakthrough loadings were observed of 1.82 and 0.22 mmol/g after thiophene (2,000 ppmw) removal from *n*-octane and benzene/*n*-octane (20 wt% C<sub>6</sub>H<sub>6</sub>), respectively. These results indicate that the adsorbent performance for sulfur removal is greatly affected by the presence of aromatics, which should occur during gasoline treatment. Moreover, since other aromatic species besides benzene can still interact with  $\pi$ -complexation adsorbents, it is important to consider the whole composition spectrum for gasoline. Table 18 shows typical aromatic composition for both the commercial gasoline and diesel. Gasoline has a considerable amount of aromatic molecules larger than benzene (because of additional functional groups), and they should compete for void space during adsorption.

Tournier et al. studied the adsorption of xylene isomers in liquid phase on a K,Ba-Y zeolite. Tournier, H.; Barreau, A.; Tavitan, B.; LeRoux, D.; Sulzer, C.; Beaumont, V. Two Experimental Methods to Study Adsorption Equilibria of Xylene Isomers in the Liquid Phase on a Y Zeolite. *Micropor. Mesopor. Mat.* **2000**, *39*, 537. For a mixture of *m*-xylene and *p*-xylene, K,Ba-Y adsorbs 0.13 mmol/g of the latter for an equilibrium concentration (liquid phase) is 2.4 mole%. This provides additional evidence that aromatics will compete for adsorption sites, even within themselves. However, even in the presence of compounds such as xylenes, Cu(I)-Y still offers considerable selectivity towards the sulfur in gasoline and this has to be due to  $\pi$ -complexation. One gram of adsorbent is capable of producing 14 cm<sup>3</sup> of sulfur free gasoline (< 1 ppmw S), removing thiophenes and benzothiophenes (BTs), and their substituted counterparts.

Figure 36 depicts the evolution of each sulfur species downstream Cu(I)-Y as determined by GC-FPD analyses. Breakthrough curves for selected gasoline sulfur compounds (Figure 37) were obtained also from the GC-FPD data. The chromatograms show the adsorbent has selectivity towards substituted thiophenes and heavier molecules over non-substituted molecule. This can be observed in the relative intensities of the peaks in the 4 minutes (elution time) region (please refer to Figure 33 for peaks reference. Most substituted thiophenes and BTs remain highly unreacted during conventional HDS processes, which is clearly not the case when using  $\pi$ -complexation zeolites.

One alternative to increase both breakthrough and saturation capacities is to provide a guard bed to take care of the aromatics during the  $\pi$ -complexation process with Cu(I)-Y. PCB type activated carbon (AC) was chosen to accomplish this. PCB-AC is

used commercially for both liquid- and vapor-phase applications including recovery of alcohols, hydrocarbons and aromatics. The present inventors performed vapor-phase single component equilibrium adsorption experiments for thiophene and diesel in PCB-AC. More benzene than thiophene was adsorbed even at pressures below  $1 \times 10^{-2}$  atm, which indicates polarizability plays an important role in the performance of this adsorbent. A similar behavior should be observed also in liquid-phase adsorption. Choma et al. studied how to predict solute adsorption behavior from liquid-phase adsorption on carbons based on the corresponding gas/solid adsorption parameter, and vice-versa. Choma, J. Burakiewicz, Mortka, W.; Jaroniec, M.; Gilpin, R.K. Studies of the Structural Heterogeneity of Microporous Carbons Using Liquid/Solid Adsorption Isotherms. *Langmuir* **2000**, *39*, 537. They demonstrated, for both types of interfaces, that similar information about the structural heterogeneity of the adsorbent may be gathered. It should be mentioned that their results were obtained for benzene as solute.

For the experiments involving activated carbon, the guard bed was loaded on top of the Cu(I)-Y bed after making sure the latter was packed uniformly. The adsorbent activation procedure was identical to the one described in the experimental section. Figure 35 shows the resulting sulfur breakthrough curve for gasoline treatment after adding an activated carbon (type PCB) guard bed on top of Cu(I)-Y. The guard bed accounted for 15 wt% of the total adsorbent bed. For this experiment, the new adsorbent combination proves to enhance the sulfur removal process, indicating this the activated carbon probably offers less mass transfer resistance towards aromatics allowing for an apparent sulfur concentration wave front to move ahead faster and reach Cu(I)-Y first. During the momentary absence of aromatics, the sulfur compounds should take advantage of the  $\pi$ -complexation process since the competitive adsorption process observed for “unprotected” Cu(I)-Y is delayed. Breakthrough and saturation capacities (from Figure 35) were 0.18 and 0.50 mmol/g, respectively (Table 17). This is a 28% increase in capacity over the one offered by Cu(I)-Y without a guard bed.

It is to be understood that the guard bed may be located in any suitable position. In a non-limitative embodiment, the guard bed is located adjacent the inlet of the main bed. It is to be further understood that the guard bed may be formed from any suitable sorbent, including but not limited to activated carbon, activated alumina, silica gel, zeolites, clays or pillared clays, diatomaceous earth, any of the porous sorbents, and/or mixtures thereof.

GC-FPD analysis (Figure 38) shows that thiophene molecules breakthrough faster, possibly indicating that competitive adsorption now lies (at least for some time) within the sulfur compounds (substitutes and non-substituted) themselves. This can be seen also in Figure 39, where thiophene concentration has reached almost 60% of the

corresponding saturation value after processing about 30 cm<sup>3</sup> of gasoline per gram of adsorbent. The methyl-substituted BTs have reached 10% on their respective concentration saturation values at similar conditions.

The same adsorbent combination (AC/Cu(I)-Y) was also tested for diesel desulfurization. Figures 40, 41, and 42 show total sulfur breakthrough curves, GC-FPD chromatograms, and selected sulfur containing molecules breakthrough curves, respectively. For total sulfur removal from diesel, the breakthrough and saturation loadings are 0.32 and 0.59 mmol/g, respectively. This translates to a saturation capacity of about 1.85 wt% sulfur. The GC-FPD data and individual component breakthrough curves show the adsorbent combination has some selectivity towards specific molecules. Figure 42 shows 4,6-dimethyldibenzothiophene molecules leaving the bed early, but not in considerable fashion. This behavior could be due to pore clogging with some substituted dibenzothiophenes. However, this is not expected since Y zeolite is known to adsorb substituted aromatics molecules in considerable quantities. For example, at  $P/P_o = 0.5$ , X zeolite (FAU, Si/Al = 1.33) adsorbs 43.3 benzene molecules and about 37 toluene molecules per unit cell, respectively. Na-X (Si/Al = 1.25) also adsorbs larger molecules such as (C<sub>4</sub>H<sub>9</sub>)<sub>3</sub>N (~16 molecules per unit cell), which has a kinetic diameter of  $s = 8.1$  Å. Thus, pore clogging in Cu(I)-Y may occur for heavily substituted dibenzothiophenes and in the presence of framework faults, specially those affecting pore window locations.

When comparing treatment results for both gasoline and diesel and the same adsorbent combination (i.e. Cu(I)-Y with a guard bed) it is believed that the fuel composition (other than the sulfur content) plays an important role in the adsorbent performance. Since, as discussed above, the amount of aromatics is believed to play an important role in diminishing the sulfur removal capacity (i.e. aromatics will also do  $\pi$ -complexation with copper cations), differences in aromatic content between different fuels should be taken into consideration. Although Table 18 shows some aromatics such as benzene as not as abundant in diesel than in gasoline, an estimate of total aromatic content is in place.

C-H bond stretching for both aromatics and aliphatics is sometimes straightforward to identify from FTIR spectroscopy. C-H stretching for alkyl, alkenyl, and aromatics shows intensities in the 2853 – 2962, 3010 – 3095, and ~3030 cm<sup>-1</sup> regions, respectively. IR intensities are usually strong for the first and third regions, while for the second case these are of a moderate type. Figure 43 presents FTIR spectra for the gasoline and diesel used during this study. From a qualitative perspective, it is clear the C-H bond stretching relative intensities are stronger near the aromatic range for gasoline, while diesel shows a stronger signal in the aliphatic region. An estimate of the aromatic/aliphatic composition was obtained after integrating the spectra for the regions just mentioned. The

total aromatic content for gasoline and diesel was estimated to be 33.7 and 24.7%, respectively. Thus, since linear molecules (such as alkanes) are not expected to compete during adsorption, less aromatics should favor sulfur removal with Cu(I)-Y or AC/Cu(I)-Y.

The present inventors were able to completely regenerate Cu(I)-Y zeolites after saturating them with thiophene molecules removed from liquid hydrocarbons. They found that using air at 350°C provides a suitable way to completely remove the sulfur containing molecules completely. After this treatment, the adsorbent needs to be auto-reduced in an inert atmosphere to recover its activated form. It is believed the same regeneration scheme may be used after treating gasoline or diesel, but the adsorbent adsorption capacity is enough to consider the use of disposable units for on-board applications.

**Table 16. Composition data for Cu(II)-Y and Na-Y zeolites obtained from neutron activation analysis (NAA).**

Adsorbent	Molar Ratios		
	Na/Al	Cu/Al	Si/Al
Na-Y	0.94	--	2.43
Cu(II)-Y	0.28	0.36	2.43

**Table 17 . Breakthrough and saturation loadings for gasoline or diesel total sulfur in Cu(I)-Y zeolites.**

Fuel Type	Average Sulfur Content (wt%)	Adsorbent	Breakthrough Loading (mmol/g)	Saturation Loading (mmol/g)
Gasoline	335	Cu(I)-Y	0.14	0.39
		AC/Cu(I)-Y**	0.18	0.50
Diesel	430	AC/Cu(I)-Y**	0.34	0.59

\*\* Adsorbent bed made of two layers: top is PCB type activated carbon (AC) and bottom is Cu(I)-Y zeolite. AC accounts for 15 wt% of the bed weight.

**Table 18. Typical aromatic composition of some commercial fuels. Average values are shown in parentheses.**

Fuel Type	Typical Composition (vol%)					
	Total Aromatics	Benzene	Toluene	Xylene	Ethylbenzene	Cumene
Gasoline	12.8 – 56.7 (30.7)	0.4 – 3.48 (1.16)	1.5 – 16.8 (7.0)	0.8 – 8.4 (4.0)	0.36 – 2.63 (1.36)	0.04 – 0.17 (0.08)
Diesel	15.7 – 47.2 (31.8)	0 – 0.02 (0.01)	0 – 0.18 (0.05)	0.04 – 0.71 (0.15)	0.02 – 0.7 (0.04)	0.01 – 0.06 (0.02)

*Note: Data available from British Petroleum (BP), 2001 TRW Summer Motor Gasoline Survey Report, and AAM Diesel Fuel Surveys.*

## EXPERIMENT F

After activating the adsorbents *in-situ*, gasoline was passed through the fixed-bed, and the sulfur concentration in the effluent was monitored as a function of time. Fig. 44 shows the breakthrough curve obtained during desulfurization of gasoline with a Cu(I)-Y adsorbent. Adsorption capacities at both breakthrough (i.e., the break point, or the first point with detectable sulfur) and saturation were obtained upon integration of the area above the breakthrough curve. For gasoline treatment with Cu(I)-Y, the loadings at breakthrough and saturation were 0.14 and 0.39 mmol/g, respectively (Table 17). From Fig. 44, one gram of Cu(I)Y was capable of producing 14 cm<sup>3</sup> of sulfur free gasoline (< 0.28 ppmw S), removing thiophenes, benzothiophenes (BTs), and their substituted counterparts. Fig. 44 also shows the resulting sulfur breakthrough curve for gasoline after adding an activated carbon (type PCB) guard bed on top of Cu(I)-Y. The guard bed accounted for 15 wt% of the total adsorbent bed. For this run, the new adsorbent combination proved to significantly enhance the sulfur removal capacity. The breakthrough and saturation capacities (from Fig. 44) were 0.18 and 0.50 mmol/g, respectively (Table 17).

Fig. 45 depicts the evolution of each sulfur species in the adsorber effluent as determined by GC-FPD analyses. The chromatograms show the adsorbent has selectivity towards substituted thiophenes and heavier molecules over non-substituted molecules (i.e., thiophene). This can be observed from the relative intensities of the peaks in the 4-minute (elution time) region.

## EXPERIMENT G

Nickel (II) based sorbents were used for the desulfurization of commercial diesel fuels via  $\pi$ -complexation.

**Adsorbent Preparation.** The sorbents were prepared by ion-exchange. Na-Y zeolite (Si/Al = 2.43, Strem Chemicals), NH<sub>4</sub>-Y zeolite (Si/Al = 2.40, Strem Chemicals), and 13-X zeolite (Si/Al = 1.25, Linde), all in powder form, were used as starting adsorbent materials. H-Y zeolites were obtained after calcination of NH<sub>4</sub>-Y with air at 450°C.

The sorbents were modified by either liquid phase (LPIE) or solid-state ion (SSIE) exchange techniques. Ni(II)-Y(LPIE) and Ni(II)-X(LPIE) were prepared by ion exchanging Na-Y and 13-X, respectively, with NiCl<sub>2</sub> 6H<sub>2</sub>O aqueous solutions for 48 hours at either RT or 135°C. For Ni(II)-X(LPIE), the zeolite and aqueous solutions were placed in an autoclave and heated to a desired temperature. During the ion exchange process at RT the pH was kept at a value of approximately 6 to avoid hydrolysis of the nickel(II) species in solution. After ion exchange, the powder crystals were recovered by filtration

and washed with about 4 liters of deionized water to remove excess  $\text{NiCl}_2$ . The sorbents were dried at  $90^\circ\text{C}$  for 24 hours and stored in sealed vials. The exchanged zeolites, which were white powders initially, were green at the end of the nickel ion exchange process.

5  $\text{NH}_4\text{-Y}$  zeolite was ion exchanged twice using  $\text{Ce}(\text{NO}_3)_3$  aqueous solutions at  $80^\circ\text{C}$ . The final product was also recovered by filtration and washed with copious amounts of deionized water.

The SSIE method may be used to obtain zeolites with high nickel content. This method may advantageously allow metal cations to be introduced into extra-framework positions without the presence of hydrolyzed species that may result from aqueous exchanges.

10  $\text{H-Y}$  zeolites and  $\text{NiCl}_2 \cdot 6\text{H}_2\text{O}$  were manually mixed. The amount of nickel(II) used corresponded to the maximum theoretical cation exchange capacity (CEC) for the zeolite. Afterwards, the powder/salt mixture was placed inside a reactor, was heated from RT to  $150^\circ\text{C}$  at  $1^\circ\text{C}/\text{min}$ , and was held at that temperature for about 4 hours, all in a dry oxygen atmosphere. The temperature was then increased to  $500^\circ\text{C}$  also at  $1^\circ\text{C}/\text{min}$  and held at that set point for period ranging between about 6 and about 12 hours. The oxygen gas was pre-treated for moisture removal using 3-A type zeolite beds. The gas flow rate was kept constant at about  $140 \text{ cm}^3/\text{min}$ . After heating, the zeolite was allowed to slowly cool down to RT also in dry oxygen.

20 **Reagents and Standards.** Commercial samples were obtained from a gas station located in Ann Arbor, MI. The actual sulfur content was measured by gas chromatography techniques. Thiophene, benzothiophenes (BT), dibenzothiophene (DBT) standards were purchased from Sigma-Aldrich.

25 **Elemental Analysis.** The nickel(II) sorbents were characterized using neutron activation analysis (NAA) in the research nuclear reactor of the Radiation Center at Oregon State University following standard procedures.

30 **Fixed-Bed Adsorption/Breakthrough Experiments.** The dynamic adsorption or breakthrough experiments were performed in vertical custom made quartz adsorbers equipped with a supporting glass frit. The setup consisted of a low-flow liquid pump, Kynar compression fittings, feed tanks, and a heating element. Initially, the sorbents were loaded inside the adsorber, and heated *in situ* using dry gases to avoid exposure to atmospheric moisture. The nickel-based sorbents were heated to  $350^\circ\text{C}$  at  $1^\circ\text{C}/\text{min}$  in an inert gas atmosphere and held at that temperature for at least 18 hours. The  $\text{Ce(III)-Y}$  zeolite sorbent was heated to  $450^\circ\text{C}$  in dry air at  $2^\circ\text{C}/\text{min}$  and held at that temperature for 6

hours. The gases used for activation were pretreated inline before contacting the sorbent using a 3A-type zeolite. After activation treatment, the nickel and cerium zeolites were allowed to cool down to RT and 80°C under gas flow and then were tapped to ensure proper packing. The feed was switched to a commercial grade gasoline or diesel and effluent samples were collected at regular intervals until saturation was achieved, which depended on the adsorption dynamics and the amount of adsorbent.

The nickel and cerium zeolites were regenerated at 350°C and 450°C, respectively. Dry air was used for calcination regeneration test and the temperature was controlled by a PID temperature controller within + 1°C.

**Gas Chromatography Analysis.** The samples' sulfur content was analyzed as described in Experiment E. Thiophene, BT and DBT standard solutions were diluted in sulfur-free *n*-octane to a known concentration and then injected for retention time determination. Using thiophene, BT and DBT, it was established that the peak area per S was statistically the same for these three molecules at similar sulfur concentrations. After obtaining calibration data at different concentration levels, the diesel fuel total sulfur content was estimated by carefully adding up all individual peaks areas. The total sulfur content of the fuel was 297.2 ppmw-S. Figure 46 shows a detailed FPD chromatogram for the diesel fuel tested. Detectable thiophenic sulfur peaks from standards were recorded at concentrations down to approximately 20 ppbw S (or 50 ppbw thiophene).

**Nitrogen Equilibrium Adsorption Isotherms.** Some of the sorbents were tested for surface area measurements. This information was obtained from liquid nitrogen (at about 196°C) equilibrium isotherms and following standard procedures. The equilibrium data was gathered using a Micromeritics ASAP 2010 static volumetric analysis unit.

## Results and Discussion

**Adsorbent Characterization.** Characterization for the adsorbents were achieved by NAA. All the zeolites were in hydrated conditions before testing. As seen in Table 19, ion-exchanging Na-Y with aqueous solutions containing Ni<sup>2+</sup> species resulted in incomplete ion exchange. If it is assumed that one Ni<sup>2+</sup> cation compensates for two aluminum tetrahedral charges, then in the present case the ion exchange resulted in 50 and 62% substitution of the original sodium ions for Ni(II)-Y (LPIE-RT) and Ni(II)-Y (LPIE-

135), respectively. The remaining sodium ions were compensating for the other aluminum tetrahedra charges; in other words, the  $(2\text{Ni} + \text{Na})/\text{Al}$  ratio should be unity. For the sample using solid-state exchange techniques, the exchange was complete (i.e.,  $2\text{Ni}/\text{Al} = 1.0$ ) as expected.

5 **Table 19. Composition data for sorbents obtained from neutron activation analysis (NAA). Unit cell composition given for dehydrated zeolites.**

Molar Ratios			
Adsorbent	2Ni/Al	Si/Al	Unit Cell Composition
Ni(II)-Y (LPIE-RT)	0.50	2.43	$\text{Ni}_{14}\text{Na}_{28}(\text{Al}_{56}\text{Si}_{136}\text{O}_{384})$
Ni(II)-Y (LPIE-135)	0.62	2.43	$\text{Ni}_{18}\text{Na}_{20}(\text{Al}_{56}\text{Si}_{136}\text{O}_{384})$
Ni(II)-Y (SSIE-500)	1.00	2.40	$\text{Ni}_{29}(\text{Al}_{57}\text{Si}_{135}\text{O}_{384})$
Ni(II)-X (LPIE-RT)	0.38	1.25	$\text{Ni}_{17}\text{Na}_{52}(\text{Al}_{86}\text{Si}_{106}\text{O}_{384})$

10 **Fixed-Bed Adsorption Experiments.** After *in situ* activation of the adsorbent bed, a commercial diesel feed (297 ppmw-S) contacted the beds and the effluent total sulfur content was monitored periodically. *In situ* activation was necessary for evaluation of the sorbents desulfurization capabilities without any exposure of the hydrophilic zeolites to atmospheric air. After activation, the nickel(II) zeolites were pink in color, as opposed to the greenish color observed after ion exchange, which indicated the sorbents were  
 15 dehydrated. Breakthrough adsorption curves were generated by plotting the transient total sulfur concentration normalized by the feed total sulfur concentration versus cumulative fuel volume normalized by total bed weight. The adsorption amounts (normalized per adsorbent weight) were obtained after solving the following equation

$$20 \quad q_{\text{breakthrough or saturation}} = \left( \frac{\dot{V}}{m_{\text{adsorbent}}} \right) \left( \frac{\rho_{\text{fuel}} C_i}{MW_{\text{sulfur}}} \right) \int_0^t \left[ 1 - \frac{C(t)}{C_i} \right] dt \quad (11)$$

where  $\nu$  is feed volumetric flow rate ( $\text{cm}^3/\text{min}$ ),  $\rho_{\text{fuel}}$  is the fuel density at RT,  $C_i$  is the total sulfur concentration in the feed (ppmw-S),  $m_{\text{adsorbent}}$  is the weight of the sorbent bed (g),  $MW_{\text{sulfur}}$  the molecular weight of sulfur,  $C(t)$  the effluent total sulfur concentration (ppmw-S) at any time  $t$  (min). The integral part on the right hand side of eq 11 is the area above the breakthrough curves. Table 20 summarizes the results obtained for total sulfur  
 25 breakthrough and saturation adsorption amounts in fresh activated sorbents.



**Table 20. Breakthrough loadings for total sulfur from diesel on fresh sorbents.**

Adsorbent	Breakthrough Loading (mmol/g) <sup>b</sup>	Saturation Loading (mmol/g) <sup>b</sup>
Ni(II)-Y (LPIE-RT)	0.085	0.204
Ni(II)-Y (LPIE-135)	0.120	0.213
Ni(II)-Y (SSIE-500)	0.158	0.289
Selexsorb CDX/ Ni(II)-Y (SSIE-500) <sup>a</sup>	0.191	0.331
Ni(II)-X (LPIE-RT)	0.143	0.251
Selexsorb CDX/ Ni(II)-X (LPIE-RT) <sup>a</sup>	0.161	0.281
Ce(IV)-Y (LPIE-80)	0.043	0.122

<sup>a</sup> Adsorbent bed contained two layers: the first layer was alumina Selexsorb CDX (CDX) followed by Ni(II)-Y or Ni(II)-X zeolite. CDX accounts for 25 wt% of the bed weight.

<sup>b</sup> Loading amounts normalized by total bed weight.

Figure 47 shows the resulting breakthrough curves for Ni(II)-Y (LPIE-RT) and Ni(II)-X (LPIE-RT) beds. The zeolites are capable of deep desulfurizing (e.g. total sulfur content less than 1 ppmw) about 11.44 and 19.24 cm<sup>3</sup> of diesel per gram of sorbent, respectively, corresponding to adsorption of 1.10 and 1.94 thiophenic molecules per zeolite unit cell, respectively. For both sorbent cases, sulfur saturation loading is reached after processing approximately 70 cm<sup>3</sup> of diesel per gram of sorbent. Recent reports on jet fuel desulfurization with Ni(II)-Y containing 4 nickel ions per unit cell indicate the zeolite is capable of removing 0.08 mmoles of thiophenic sulfur per gram of zeolite at saturation. Although diesel instead of jet fuel was tested in the present case, the aforementioned value is orders of magnitude lower than the amount obtained with our Ni(II)-Y (LPIE-RT), which is about 0.20 mmoles per gram of zeolite (see Table 20). The organosulfur species present in jet fuel are mostly substituted and non-substituted benzothiophenes. Diesel also contains refractory dibenzothiophenes, which may be difficult to remove. The sorbent in this example has 14 nickel ions per unit cell, 71% more ions than the zeolite used for the jet fuel desulfurization work. This difference accounts for such difference in adsorption capacities.

The desulfurization performance differences observed in Figure 47 may be the result of the zeolites ion exchange characteristics. Since X-type (Si/Al = 1.25) zeolites have 54% more cation sites than Y-type (Si/Al = 2.43) zeolites, the former were expected to offer more exposed nickel(II) ions and, as a result, higher adsorption capacities. For thiophenic molecules to be adsorb, this has to occur in the zeolite supercages and the cation sites exposed to these are (following the Smith nomenclature, Smith, 1971, cited above) site II (SII), site III (SIII), site III' (SIII') and site U (SU). Cation sites for faujasite zeolites are portrayed in Figure 48. Few zeolites have been identified to possess sites SU, (See Breck, cited above) and this has not observed for nickel(II) exchanged zeolites. X-ray

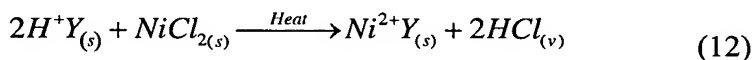
diffraction studies for aqueous phase nickel(II) exchanged Y zeolites showed the nickel cations prefer sites SI, SI', SII, and SII. No site SIII occupancy was ever observed. Additionally, nickel ions in activated Ni(II)-zeolites occupy exposed sites when the cation content in the zeolite was greater than 12 cations per unit cell. Nevertheless, mobility of the cations of  $\text{Ni}^{2+}$  ions to exposed sites upon adsorption of molecules has been studied before. Pyridine adsorption on Ni(II)-Y zeolites dehydrated at  $300^\circ\text{C}$  causes nickel ions located in hexagonal prism windows (SI') to migrate because of strong interactions with aromatic rings. This is also expected to occur when adsorbing thiophenic rings on Ni(II)-zeolites particularly because of the strong  $\pi$ -complexation mechanism. For the case of aqueous phase exchanged Ni(II)-X zeolites, Bae and Seff found nickel ions preferentially occupy sites SII and SIII'. Thus, the cation positions in X-zeolites seem to favor adsorption of thiophenic molecules as shown in Figure 47. The nickel (II) zeolites changed from the color pink to brown during the desulfurization process. It is to be understood that the color change may be gradual and along the length of the bed.

Figures 49A and 49B show breakthrough adsorption of specific organosulfur molecules during desulfurization of a commercial diesel also with Ni(II)-Y (LPIE-RT) and Ni(II)-X (LPIE-RT) beds, respectively. Both zeolites are capable of removing refractory thiophenic compounds (e.g. 4-methyldibenzothiophene (4-MDBT), 4,6-dimethyldibenzothiophene (4,6-DMDBT) and 2,4,6-trimethyldibenzothiophene (2,4,6-TMDBT)), which remain largely intact during traditional HDS processes. However, the exposed cations in Ni(II)-X (LPIE-RT) zeolites are capable of removing the organosulfur molecules without much discrimination between them, largely due to  $\pi$ -complexation interaction between the exposed cation and the aromatic rings. Thus, substituted thiophenic rings with methyl groups surrounding the sulfur atom may also be easily removed, as opposed to HDS, which relies on attacking the sulfur atom directly. The sodium ions remaining in the zeolite structure after ion exchanging Na-X and -Y zeolites for nickel are not responsible for the deep-desulfurization process, because Na-Y zeolites are not capable of deep-desulfurizing liquid fuels due to of the lack of  $\pi$ -complexation capability.

In order to increase the adsorption capacity and the selectivity of Ni(II)-Y, other methods to increase the concentration of nickel ions per unit cell were tested. One method was to increase the ion exchange temperature. Olson (1968) ion exchanged faujasite zeolites with nickel (II) ions to almost 100% capacity by using a temperature of  $90^\circ\text{C}$  and for 60 days. A higher exchange temperature may accomplish the work in a smaller time window. Figure 50 shows the resulting diesel desulfurization breakthrough curves for a zeolite prepared after ion exchanging Na-Y with nickel(II) at  $135^\circ\text{C}$ . Ni(II)-Y (LPIE-135) shows a considerable increase in total sulfur adsorption loading before

breakthrough occurs. The capacity increased by 41% when compared to the one obtained with Ni(II)-Y (LPIE-RT) (refer to Table 20). This corresponds to approximately 1.55 organosulfur molecules per zeolite unit cell. These results clearly indicate that more nickel(II) ions were added to extra-framework positions and were located in exposed sites. Ion exchange at higher temperatures to obtain high nickel loadings in X-zeolites resulted in the collapsing of the framework as determined from nitrogen adsorption at  $-196^{\circ}\text{C}$ . The surface area was approximately  $200\text{ m}^2/\text{g}$ , which may indicate crystallinity loss and, thus, the sorbent was not tested for desulfurization. Donghan and Seff observed the collapse of Co(II)-X zeolites caused by exchange at high temperatures. The same may be occurring during exchange for  $\text{Ni}^{2+}$  into X-zeolite at high temperatures.

The SSIE technique may be an excellent way of exchanging cations in a more direct fashion. The advantages of SSIE over conventional ion exchange from aqueous media may generally include: (i) absence of large volumes of salt solution, (ii) avoiding the problem of discarding waste salt solution, and (iii) allowing metal cations (which are small) to be introduced through narrow windows or channels that would impede or prevent ion exchange of solvated cations (which are larger) from aqueous solution. The SSIE process to obtain Ni(II)-Y involves the following reaction scheme:



The H-Y zeolite and Ni(II)Cl were mixed thoroughly and heated in dry air, oxygen, or vacuum to induce the ion exchange. Thorough mixing of the solid species is crucial for successful ion exchange, but this could be detrimental to the zeolite framework if not performed carefully. For the present invention, the zeolite and nickel source were mixed by hand without applying any pressure to the powders. After SSIE of H-Y with  $\text{NiCl}_2$  to obtain Ni(II)-Y (SSIE-500), the final sorbent was used to desulfurize a fresh diesel feed and the results are shown on Figure 50.

Ni(II)-Y (SSIE-500) is capable of deep-desulfurizing approximately  $22\text{ cm}^3$  of diesel per gram of sorbent. This corresponds to a 10, 32, and 85% increase in breakthrough loading when compared to Ni(II)-Y (LPIE-RT), Ni(II)-Y (LPIE-135), and Ni(II)-X (LPIE-RT), respectively. As shown in Figure 51A, the SSIE zeolite removed all compounds without distinction among the different organosulfur molecules present in the diesel, including the refractory compounds. SSIE to obtain Ni(II)-X was not tried because of the low thermal stabilities of zeolites containing high concentration of aluminum atoms per unit cell. (see Breck, 1984, cited above).

Velu, Ma, and Song claimed fuel desulfurization via chemical adsorption using cerium-exchanged zeolites. The process involved direct interaction with the sulfur atoms of the thiophenic molecules and was tested for desulfurization of model jet fuel at 80°C. Cerium exchange Y-zeolites (Ce-Y) were prepared (based on this literature) and tested for desulfurization of a commercial diesel fuel. The sorbent was activated in dry air at 450°C and the fuel desulfurization performed at 80°C. The elevated temperature may be necessary because the process relies on chemical reaction. After the activation and desulfurization steps, the sorbent color was yellowish and amber. The yellow color corresponds to cerium (IV) (referred to as Ce(IV)-Y (LPIE-80)). The amber color obtained after desulfurization may be indicative of a complexation mechanism. The total sulfur breakthrough curve for diesel treatment with Ce(IV)-Y (LPIE-80) is shown in Figure 50. Integration of the area above the curve indicates that the sorbent is capable of 0.013 and 0.122 mmoles of thiophenic sulfur per gram zeolite at breakthrough and saturation, respectively. For a “model jet fuel” this zeolite was capable of removing 0.072 mmoles of thiophenic sulfur per gram of zeolite under the same conditions used for the diesel treatment. The lower desulfurization capacity observed for diesel treatment may be due to a lack of interaction between the cerium ions and the sulfur atom in the refractory sulfur compounds, which are abundant in the diesel fuel (see Figure 46). In these compounds, the sulfur may be difficult to access because of steric hindrance imposed by the methyl groups adjacent to the sulfur atom. Further evidence of this comes from Figure 51B, which shows breakthrough of individual organosulfur molecules during the diesel desulfurization. The figure shows clearly that the Ce(IV)-Y (LPIE-80) sorbent has more selectivity towards non-substituted thiophenes (e.g. BT and DBT) over the substituted ones. Abundant refractory compounds such as 4,6-DMDBT leave the bed almost instantly when compared to BT and DBT.

**Layered Beds.** The best two sorbents tested here, Ni(II)-Y (SSIE-500) and Ni(II)-X (LPIE-RT), were also tested with alumina guard beds.

Figure 52 shows diesel desulfurization breakthrough curves after treatment with Selexsorb CDX/Ni(II)-Y (SSIE-500) and Selexsorb CDX/ Ni(II)-X (LPIE-RT), respectively. In all cases, the activated alumina accounted for 25 wt% of the total bed weight. A summary of the breakthrough and saturation adsorption loading capacities for

these sorbents is shown on Table 20. For both sorbents, the adsorption capacities increased when compared to the case without guard bed. The Selexsorb CDX/Ni(II)-Y (SSIE-500) matrix had the greatest adsorption capacity. Figure 53 shows the resulting adsorption breakthrough behavior of individual organosulfur compounds in a Selexsorb CDX/Ni(II)-Y (SSIE-500) layered bed. This bed adsorbed more of these compounds, and did so in a selective fashion, than did the Ni(II)-Y (SSIE-500) bed alone. Actual sulfur levels attained during desulfurization with all the nickel(II) zeolites and the layered beds are shown on Figure 54. One gram of Ni(II)-Y (SSIE-500) is capable of producing about 14 cm<sup>3</sup> of diesel fuel with a sulfur content of 0.256 ppmw-S, which may be suitable for use in fuel cell reforming units. The same zeolite, when coupled with activated alumina Selexsorb CDX, is capable of producing about 19 cm<sup>3</sup> of diesel fuel with a sulfur content of 0.220 ppmw-S (Figure 55).

**Sorbent Regeneration.** Ni(II)-Y (SSIE-500) was tested for regeneration after saturation with diesel organosulfur molecules. The regeneration was achieved in a single step: calcination in dry air at 350°C for about 6 hours. After calcination, the sorbent recovered its original pink color. Afterwards, a fresh untreated diesel feed was allowed to contact the sorbent at RT (RT) and the 2<sup>nd</sup> desulfurization cycle monitored for sulfur elution. Figure 56 shows the total sulfur adsorption breakthrough curve and compares it the 1<sup>st</sup> cycle results. The regeneration scheme was capable of recovering all of the original sulfur sorption capacity in one step.

Figure 57 shows diesel desulfurization breakthrough curves for the regenerated Ce(IV)-Y (LPIE-80). The sorbent was regenerated under the same conditions used for its activation (e.g. using dry air at 450°C for 6 hours). A second desulfurization cycle shows the sorbent adsorption capacity diminished by 74% (see Table 21), which may be due to strong interactions of cerium ions with the adsorbed organosulfur or to low zeolitic framework stability with Ce cations.

**Table 21. Breakthrough and saturation loadings for total sulfur from diesel on regenerated sorbents.<sup>a</sup>**

Adsorbents	Regeneration Method	Stage	Breakthrough Loading (mmol/g)	Saturation Loading or Total Sulfur Removed (mmol/g)	Sorbent Breakthrough Capacity Recovery (%) <sup>c</sup>
Ni(II)-Y (SSIE-500)	Air <sup>b</sup>	2 <sup>nd</sup> Cycle <sup>d</sup>	0.157	0.275	99.4
Ce(IV)-Y (LPIE-80)	Air <sup>c</sup>	2 <sup>nd</sup> Cycle <sup>d</sup>	0.032	0.091	74.4

<sup>a</sup> Refer to Table 2 for fresh adsorbent breakthrough loading capacities.

<sup>b</sup> Regeneration in air at 450°C for 6 hours.

<sup>c</sup> Regeneration in air at 350°C for 6 hours.

<sup>d</sup> 2<sup>nd</sup> cycle desulfurization with fresh un-treated diesel fuel feed.

<sup>e</sup> Recovery calculated as follows:

$$\text{Recovery}\% = 100 \times ((2^{\text{nd}} \text{ cycle breakthrough loading}) / (1^{\text{st}} \text{ cycle breakthrough loading}))$$

**Conclusion.** Nickel(II) exchanged zeolites may be superior adsorbents for removal of all sulfur compounds from commercial diesel fuels, based on dynamic fixed-bed adsorption experiments. When used with a guard bed, solid state ion exchanged Ni(II)-Y may provide the best adsorption capacities both at breakthrough point and at saturation. For alumina acting as a guard bed, the process is capable of processing 19 cm<sup>3</sup>/g of diesel with an average sulfur content of 0.220 ppmw. Desulfurization tests with Ce(IV)-Y zeolites show that the sorbents have only selectivity towards non-substituted thiophenes, which are not abundant in diesel fuels. The adsorption limitations are due to lack of direct sulfur-metal interaction with refractory compounds. Nickel exchanged zeolites interact via  $\pi$ -complexation with thiophenic aromatic rings instead of attacking sulfur atoms directly.

### EXAMPLES OF SOME SUITABLE ADSORBENTS

A brief description of some non-limitative examples of adsorbents which may successfully be used in the present invention follows. Detailed descriptions may be found in U.S. Patent No. 6,423,881, and in U.S. Patent No. 6,215,037, each of which patents is incorporated herein by reference in its entirety.

The adsorbent comprises a carrier having a surface area, the carrier having dispersed thereon a monolayer of a metal compound, a non-limitative example of which is a silver compound. The metal compound releasably retains the thiophenes; and the carrier comprises a plurality of pores having a pore size greater than the effective molecular diameter of the thiophenes.

It is to be understood that any suitable carrier may be used. In a preferred embodiment, the carrier has a BET surface area greater than about 50 square meters per

gram and up to about 2,000 square meters per gram, and comprises a plurality of pores having a pore size greater than about 3 angstroms and up to about 10 microns. In a more preferred embodiment, the carrier is a high surface area support selected from the group consisting of refractory inorganic oxide, molecular sieve, activated carbon, and mixtures thereof. Still more preferred, the carrier is a refractory inorganic oxide selected from the group consisting of pillared clay, alumina and silica.

It is also to be understood that any suitable metal compound may be used. However, in a preferred embodiment, the metal compound is a silver (I) halide. In a more preferred embodiment, the metal compound is a silver salt, and the salt is selected from the group consisting of acetate, benzoate, bromate, chlorate, perchlorate, chlorite, citrate, fluoride, nitrate, nitrite, sulfate, and mixtures thereof.

In one exemplary embodiment of this embodiment of the present invention, the silver compound is silver nitrate ( $\text{AgNO}_3$ ) and the carrier is silica ( $\text{SiO}_2$ ).

The method of the present invention may further comprise the step of changing at least one of the pressure and temperature to thereby release the thiophenes-rich component from the adsorbent. It is to be understood that the pressures and temperatures used may be within a suitable range. However, in the preferred embodiment, the selected pressure of preferential adsorption is a first pressure, and the pressure of release is a second pressure less than the first pressure. In a more preferred embodiment, the first pressure is in a range of about 1 atmosphere to about 35 atmospheres, and the second pressure is in a range of about 0.01 atm to about 5 atm.

In the preferred embodiment, the selected temperature of preferential adsorption is a first temperature, and the temperature of release is a second temperature greater than the first temperature. In a more preferred embodiment, the first temperature is in a range of about  $0^\circ\text{C}$  to about  $50^\circ\text{C}$ , and the second temperature is in a range of about  $70^\circ\text{C}$  to about  $200^\circ\text{C}$ .

Without being bound to any theory, it is believed that the retaining of the thiophenes is accomplished by formation of  $\pi$ -complexation bonds between the metal compound and the thiophenes.

The  $\pi$ -complexation generally pertains to the main group (or d-block) transition metals, that is, from Sc to Cu, Y to Ag, and La to Au in the periodic table. These metals or their ions can form the normal  $\sigma$  bond to carbon and, in addition, the unique characteristics of the d orbitals in these metals or ions can form bonds with the unsaturated hydrocarbons (olefins) in a nonclassic manner. This type of bonding is broadly referred to as  $\pi$ -complexation, and has been considered for gaseous hydrocarbon separation and purification using cumbersome liquid solutions.

A further example of an adsorbent comprises an ion-exchanged zeolite selected from the group consisting of zeolite X, zeolite Y, zeolite LSX, and mixtures thereof, the zeolite having exchangeable cationic sites, and at least some of the sites have a metal or metal cation, eg., manganese cation, palladium, iron cation, cobalt cation, nickel cation, zinc cation, gallium cation, cadmium cation, silver cation or copper cation, present. Table 22 lists some of these metal and metal cations and their corresponding orbital occupancies. These cations may have empty 4s orbitals while having high occupancies in the 3d orbitals, thus may form  $\pi$ -complexation bonds with thiophenes. For a non-limitative example, nickel has the following electronic configuration:  $1s^2 2s^2 2p^6 3s^2 3p^6 3d^8 4s^0$  and thus is able to form  $\pi$ -complexation bonds with thiophenes and thiophene compounds.

**Table 22. Cations for  $\pi$ -complexation and corresponding orbital occupancies**

Cation for $\pi$ -Complexation	Cation Electronic Configuration
Mn <sup>2+</sup>	$1s^2 2s^2 2p^6 3s^2 3p^6 3d^5 4s^0$
Fe <sup>2+</sup>	$1s^2 2s^2 2p^6 3s^2 3p^6 3d^6 4s^0$
Co <sup>2+</sup>	$1s^2 2s^2 2p^6 3s^2 3p^6 3d^7 4s^0$
Ni <sup>2+</sup>	$1s^2 2s^2 2p^6 3s^2 3p^6 3d^8 4s^0$
Cu <sup>+</sup>	$1s^2 2s^2 2p^6 3s^2 3p^6 3d^{10} 4s^0$
Zn <sup>2+</sup>	$1s^2 2s^2 2p^6 3s^2 3p^6 3d^{10} 4s^0$
Ga <sup>3+</sup>	$1s^2 2s^2 2p^6 3s^2 3p^6 3d^{10} 4s^0$
Pd <sup>0</sup>	$1s^2 2s^2 2p^6 3s^2 3p^6 3d^{10} 4s^2 4p^6 4d^{10} 4f^0 5s^0$
Ag <sup>+</sup>	$1s^2 2s^2 2p^6 3s^2 3p^6 3d^{10} 4s^2 4p^6 4d^{10} 4f^0 5s^0$
Cd <sup>2+</sup>	$1s^2 2s^2 2p^6 3s^2 3p^6 3d^{10} 4s^2 4p^6 4d^{10} 4f^0 5s^0$

Without being bound to any theory, it is believed that the preferential adsorption occurs by  $\pi$ -complexation.

In an embodiment of the present invention, gasoline has been desulfurized at about 24 cc/g sorbent. Using a standard cartridge size that contains 5 kg of an embodiment of the present inventive sorbent, approximately 120 liters of gasoline may be desulfurized. For a fuel cell automobile, this advantageously translates into a driving range of about 7200 miles (or about 120 hours). The sorbent of embodiments of the present invention may also be regenerated for reuse, although this is not necessary, as the inventive sorbent is relatively inexpensive. For a conventional internal combustion engine automobile, the resultant driving range is approximately 3600 miles.

While preferred embodiments of the invention have been described in detail, it will be apparent to those skilled in the art that the disclosed embodiments may be



modified. Therefore, the foregoing description is to be considered exemplary rather than limiting, and the true scope of the invention is that defined in the following claims.

**Notation**

A = repulsive parameter for Buckingham potential

B = repulsive parameter for Buckingham potential or Langmuir constant

C = dispersive parameter for Buckingham potential or constant for D-A equation

5 D = diffusivity

E = energy

n = constant

P = pressure

q = point charge or molar adsorbed amount

10 R = van der Waals radii or gas constant

r = distance or radius

T = temperature

U = potential energy

V = volumetric adsorbed amount

15 X = equilibrium mole fraction in adsorbed phase

Y = equilibrium mole fraction in gas phase

*Greek letters*

$\alpha$  = polarizability or separation factor

$\beta$  = adjustable parameter

20  $\epsilon$  = well depth parameter for Lennard-Jones potential

$\sigma$  = distance parameter for Lennard-Jones potential

*Subscript*

i = atom site or component

j = atom site or component

25 s = saturation